Microstructural development in Al-Si powder during rapid solidification

by

Amber Lynn Genau

A thesis submitted to the graduate faculty

in partial fulfillment of the requirements for the degree of

MASTER OF SCIENCE

Major: Materials Science and Engineering

Program of Study Committee:
Iver Anderson, Major Professor
Rohit Trivedi
Palaniappa Molian

Iowa State University

Ames, Iowa

2004

Graduate College
Iowa State University

This is to certify that the master's thesis of

Amber Lynn Genau

has met the thesis requirements of Iowa State University

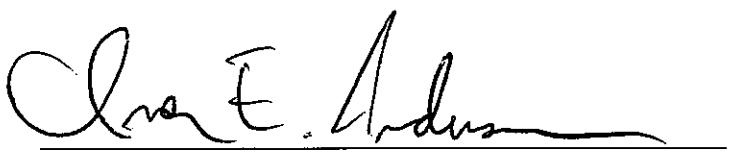

Major Professor

For the Major Program

Dedicated to Joe
who moved to Ames and
waited patiently for me
to finish this

TABLE OF CONTENTS

ABSTRACT

Powder metallurgy has become an increasingly important form of metal processing because of its ability to produce materials with superior mechanical properties. These properties are due in part to the unique and often desirable microstructures which arise as a result of the extreme levels of undercooling achieved, especially in the finest size powder, and the subsequent rapid solidification which occurs. A better understanding of the fundamental processes of nucleation and growth is required to further exploit the potential of rapid solidification processing. Aluminum-silicon, an alloy of significant industrial importance, was chosen as a model for simple eutectic systems displaying an unfaceted/faceted interface and skewed coupled eutectic growth zone. Al-Si powder produced by high pressure gas atomization was studied to determine the relationship between microstructure and alloy composition as a function of powder size and atomization gas. Critical experimental measurements of hypereutectic (Si-rich) compositions were used to determine undercooling and interface velocity, based on the theoretical models which are available. Solidification conditions were analyzed as a function of particle diameter and distance from nucleation site. A revised microstructural map is proposed which allows the prediction of particle morphology based on temperature and composition. It is hoped that this work, by providing enhanced understanding of the processes which govern the development of the solidification morphology of gas atomized powder, will eventually allow for better control of processing conditions so that particle microstructures can be optimized for specific applications.

INTRODUCTION

Today, more is being required of materials than ever before. New products and advancements demand materials that are stronger, lighter, more resistant to wear and corrosion, and capable of performing at extreme temperatures, just to name a few. New technologies, therefore, are required to produce materials that can meet these demands as well as those which will surely arise in the future. Before those technologies can be developed and perfected, however, advances in the basic understanding of fundamental material properties must be made.

Aluminum metal alloyed with silicon is one material of tremendous industrial importance. The alloy system has a number of favorable characteristics, including good wear resistance, low thermal expansion, low density and ease of welding, which make Al-Si the alloy of choice for many automotive, aerospace and electronic applications [1]. Aluminum is particularly desirable because of its low density, which reduces weight, and in cars, for example, improves gas mileage and decreases emissions. The addition of silicon as an alloying agent improves strength without significantly affecting density. Low metal forming temperatures also result in a low production cost for these parts.

Mechanical strength and wear resistance of Al-Si alloys increase with silicon content, but increasing silicon above the eutectic composition causes the formation of large, irregular silicon flakes which compromise the mechanical properties of the alloy. A number of techniques are available for refinement of primary silicon, including inoculation (grain refinement), ternary alloying and ultrasonic techniques. Another alternative is rapid solidification processing; and this seems to be the most promising route.

There are a number of methods which can be used to produce rapid solidification, including melt spinning, splat quenching, laser surface melting and several types of atomization. Of these, atomization is probably the most industrially important. This is due to its ability to process large volumes of material, a relatively high associated cooling rate, and the lack of required secondary processing steps. Melt spun ribbon, for example,

experiences a faster cooling rate, but requires a crushing step before consolidation. Spherical powder, on the other hand, can be consolidated directly, and also has better powder packing properties, which is important in applications such as bonded magnets, where the amount of magnetized powder that can be loaded into a binder is directly related to the strength of the finished magnet.

Gas atomization, whether by air, water or inert gas, accounts for the largest volumetric tonnage of powder [2]. It is commercially adaptable, and hence the most commercially available technique and utilized on the largest scale. The reason for the growing importance of powder metallurgy is two-fold: first, the ability to produce powder which can be consolidated into net shape parts requiring few, if any, finishing steps; and second, its ability to generate favorable microstructures which cannot be produced by conventional bulk ingot processing methods. These microstructures are key to improved alloy performance. In aluminum-silicon, for example, silicon content can be increased in gas atomized powders without the formation of the brittle silicon flakes.

Gas atomization also presents an opportunity to study the fundamental processes of nucleation and growth. The technique produces powder particles which can access regions of extreme undercooling. As described above, the rapid solidification which occurs at such extremes produces unique and often desirable microstructures. Gas atomization also involves containerless solidification, allowing nucleation to be studied when a substrate is not present. Aluminum-silicon provides a model system for simple binary eutectic alloys displaying an unfaceted/faceted interface during coupled growth. For comparison purposes, a large body of experimental data is available for this system, including a number of rapid solidification studies.

The gas atomization process has a large number of operating variables, including melt temperature and viscosity as the melt enters the nozzle, alloy type, metal feed rate, gas type, gas pressure, gas feed rate and velocity, nozzle geometry, gas temperature and residual atmosphere. All of these parameters are important to the final outcome of the powder, and can, to some extent, be adjusted to tailor the powder characteristics. A significant body of

work has been done at Ames Laboratory to understand and control the variables mentioned. [3,4,5].

Admittedly, the chaotic nature of gas atomization makes the study of fundamental processes somewhat challenging. There are other methods, such as electrohydrodynamic atomization, which reduce the number of variables and generate highly reproducible results, but are intended only as laboratory tools and are able to produce only a few grams of material per hour [6]. The study of gas atomized powder provides a unique combination of industrial relevance and scientific inquiry.

It has been established that there is a strong linkage between the gas atomization process conditions, the resulting powder characteristics, and the mechanical properties of the sintered compact. Trivedi et al. [7] used microhardness measurements to establish that atomized Al-Si powders with a dominant Al dendritic microstructure had a reduced strength. Kim and Suryanarayana [8] found that the properties of an extruded bar varied according to the microstructure of the constituent powder. These findings suggest an approach to design of powder compact strength by selection of powder microstructure type based on powder size and atomization parameters.

Alloy powder batches of Al-15Si and Al-18Si (wt.%) were generated at Ames Laboratory by high pressure gas atomization (HPGA), using nitrogen or helium as a fluid to break up a molten metal stream for the efficient production of very fine metal powders [9]. A vacuum induction furnace and a closed, inert gas-filled chamber were incorporated into the HPGA system to prevent oxidation of the high temperature molten alloys and the resultant droplet sprays.

The goal of the current study is to explore the relationship between microstructure and alloy composition as a function of powder size and atomization gas. Critical experimental measurements of hypereutectic compositions were used to determine exact solidification conditions, such as undercooling and interface velocity, based on the theoretical models which are available. Solidification conditions were analyzed as a function of particle diameter and distance from nucleation site. It is hoped that this work, by

providing enhanced understanding of the processes which govern the development of the solidification morphology of gas atomized powder, will eventually allow for better control of processing conditions so that particle microstructures can be optimized for specific applications.

LITERATURE REVIEW

Fundamentals of Atomized Powder

Boettinger and Perepezko [10] have done extensive studies on the nucleation and growth kinetics which govern rapid solidification processes, including atomization, and account for the phase selection which occurs in different systems. Rapid solidification is an inherent part of atomization. When a melt is broken up into many fine droplets, such as occurs during atomization, the number of droplets may exceed the number of active nucleation sites, or motes, present in the melt. After random distribution, those droplets without active nucleation sites, generally the smallest droplets, will reach significant undercoolings before nucleation occurs. This effect, known as mote isolation and illustrated in Figure 1 [11], is enhanced with extreme reduction in droplet size scale, e.g. in an atomization process, making atomized powder ideal for the study of the solidification of a deeply undercooled melt.

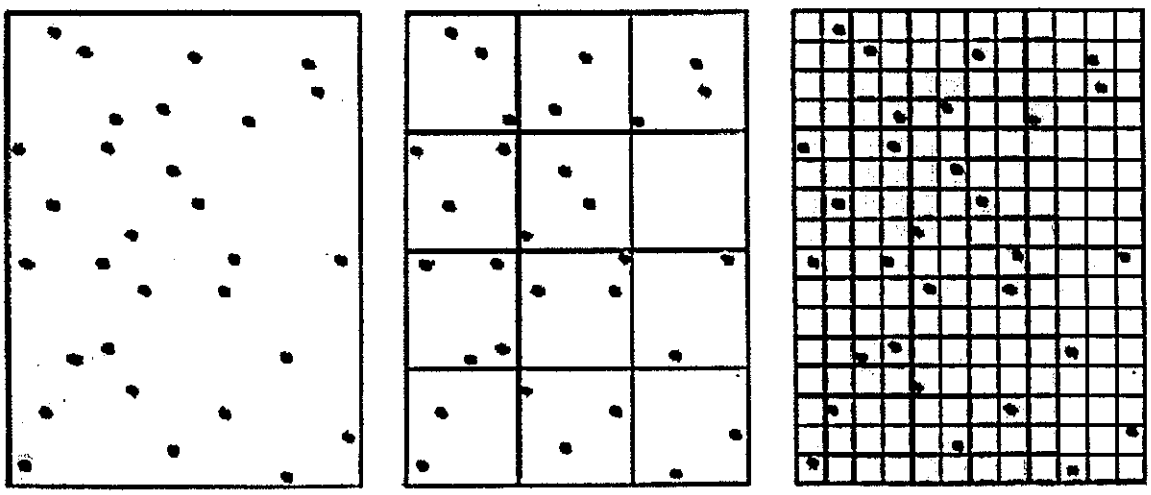

Figure 1. Illustration of mote isolation, such as occurs in atomization, where 'x' represents the mote-free fraction of each collection of volume elements.

There are several factors in the atomization process which can be varied to gain some control over the structure of the resulting powder. It has been shown by Mehrabian [12] that as the size of a gas atomized particle decreases (surface area to volume ratio increases), the convective cooling rate increases, contributing to a larger undercooling in the smaller particles. Larger undercoolings, in turn, produce a larger driving force for solidification and result in a faster interface velocity during solidification. The cooling rate of the powder during solidification can be controlled to some degree by the choice of gas used in the atomization process. A lighter gas, such as He, has a greater heat capacity and thermal conductivity, as well as a higher heat transfer coefficient, and will produce faster cooling of the particles [13]. Both of these effects are represented graphically in Figure 2.

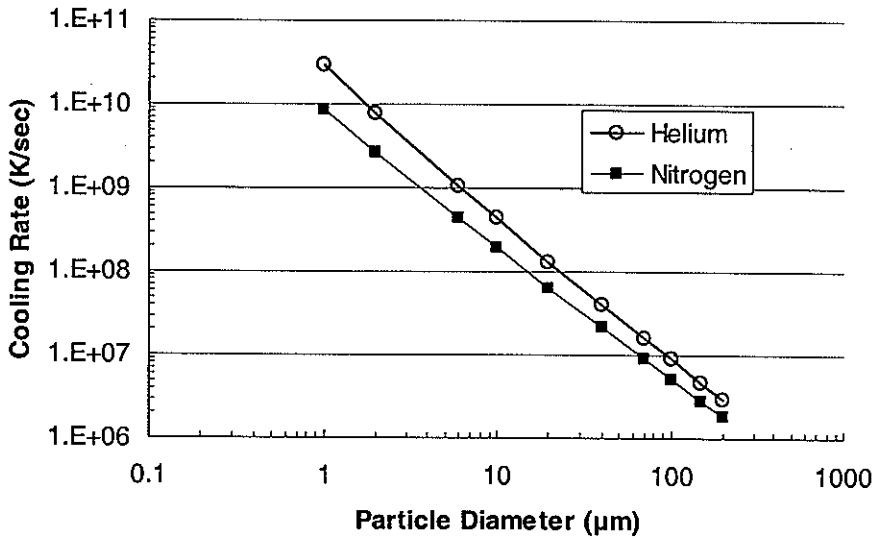

Figure 2. Calculated convective cooling rate of spherical aluminum particles for gas flowing at a velocity of Mach one, relative to the particle. Calculation based on the analysis of Mehrabian [12].

Levi and Mehrabian [14] have done extensive studies of heat flow in rapidly solidified metal droplets, developing relationships between powder processing parameters, growth kinetics, interface velocity and undercooling, and the resultant growth morphologies. They determined that there are two general regimes in the thermal history of most atomized droplets. Following path C in Figure 3, the majority of droplets first solidify adiabatically,

where most of the heat of fusion produced during recalescence is reabsorbed, increasing the temperature of the particle. The velocity of the solid/liquid interface decreases, producing a change in segregation spacing across the diameter of the droplet. There is then a transition to the second regime, were growth is slower and roughly isothermal, controlled by the rate of external heat loss. It is because of these two regimes that two separate solidification morphologies can be present in a single droplet. However, when undercooling is very large, the droplets may reach the hypercooled region (path B) where the heat of recalescence is insufficient to raise the temperature of the droplet to the T_o line. In this case, no segregation will be present in the particle.

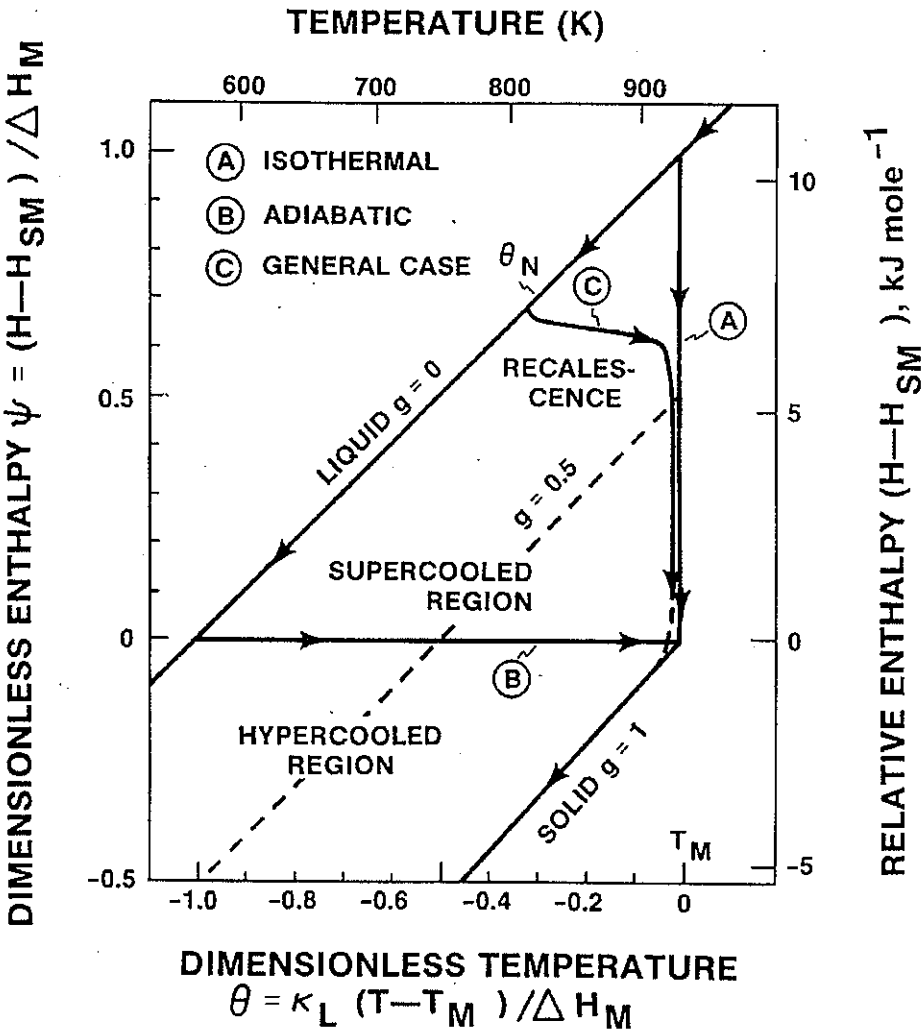

Figure 3. The effect of recalescence and possible solidification paths for Al droplets [14].

Theoretical Solidification Models

It is extremely difficult to directly measure the solidification conditions inside the atomizer chamber. However, because the microstructure varies in response to changing conditions at the interface, it can be used as an in situ probe to indirectly determine solidification conditions. Eutectic spacing, microcellular spacing and dendrite arm spacing can all be used to calculate the interface temperature and interface velocity. Eutectic spacing calculations will be considered here. The model developed by Jackson and Hunt (JH) [15] has been used for many years to relate eutectic spacing, λ, to interface velocity, V, and undercooling, ΔT, according to

$$\Delta T = K_1 \lambda V + \frac{K_2}{\lambda} \tag{1}$$

where K_1 and K_2 are system parameters which are defined as [16]

$$K_1 = \frac{mC_o}{f_\alpha f_\beta D} P_{JH} \tag{2}$$

$$K_2 = 2m \sum_i \frac{\Gamma_i \sin(\theta_i)}{m_i f_i} \tag{3}$$

where m_α and m_β are the magnitudes of the α and β liquidus slopes at the eutectic temperature, C_o is the difference in compositions of the β and α solids at the interface (i.e. length of the eutectic tie-line), D is the diffusion coefficient in liquid, f is the volume fraction of α or β phase, Γ_α and Γ_β are the Gibbs-Thomson coefficients for each phase and the angles θ_α and θ_β are shown in Figure 4. The m value is equal to $m_\alpha m_\beta/(m_\alpha+m_\beta)$, and the parameter P_{JH} is given for lamellar eutectics as [17]

$$P_{JH} = 0.338(f_\alpha f_\beta)^{1.66} \tag{4}$$

Equation 1 predicts that, at a given growth rate, the eutectic spacing will be dependant on the undercooling, as shown in Figure 5. However, the spacing will only be stable between some minimum, λ_m, and some maximum, λ_M, spacings.

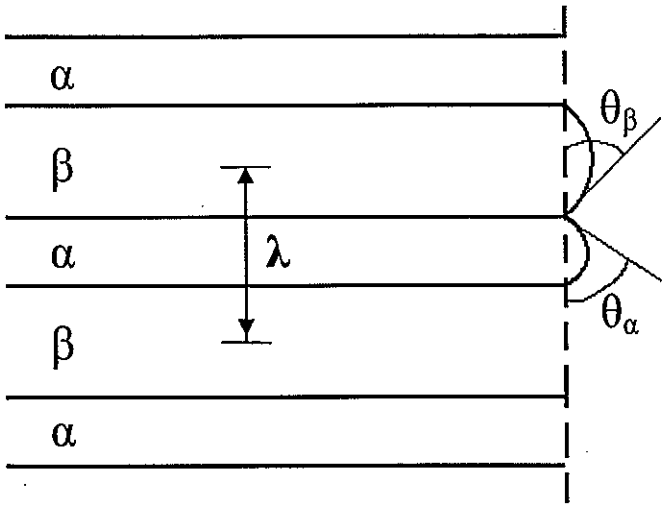

Figure 4. Schematic diagram of eutectic structure which defines the contact angles at the triple point.

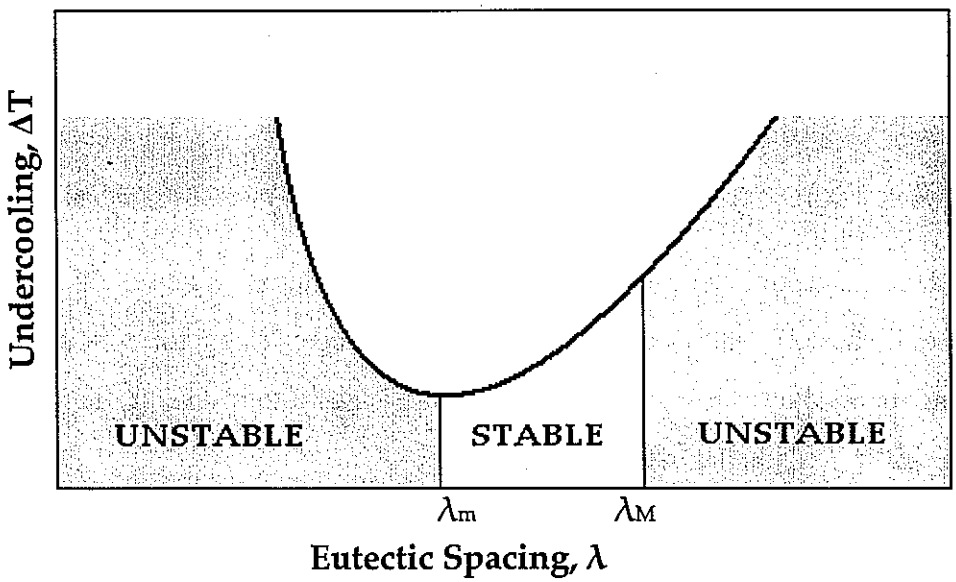

Figure 5. Relationship between the average interface undercooling and the eutectic spacing at a fixed velocity, and the regions of stable and unstable spacings.

For the maximum undercooling condition, the following relationships were calculated by Jackson and Hunt:

$$V\lambda_m^{\,2} = \frac{K_2}{K_1} \tag{5}$$

$$\Delta T\lambda_m = 2K_2 \tag{6}$$

$$\frac{\Delta T}{\sqrt{V}} = 2\sqrt{K_1 K_2} \tag{7}$$

The JH model uses the criterion that the eutectic spacing is selected at the minimum interface undercooling, which is not accurate, particularly in the Al-Si system [7]. Spacings slightly above the minimum undercooling are found to be selected instead. Jones and Kurz [18] developed a correction factor, Φ, which accounts for this deviation and remains constant for any given system. Equations 5-7 can be used to calculate undercooling and velocity from average eutectic spacing by incorporating $\Phi = \langle\lambda\rangle / \lambda_m$, where $\langle\lambda\rangle$ is the selected spacing and λ_m is the spacing corresponding to the minimum undercooling value. The following relationships can then be obtained:

$$V\langle\lambda\rangle^2 = \Phi^2 K_r / K_c = \text{constant}_1 \tag{8}$$

$$\langle\Delta T\rangle\langle\lambda\rangle = (1+\Phi^2)K_r = \text{constant}_2 \tag{9}$$

$$\langle\Delta T\rangle / \sqrt{V} = (\Phi + \frac{1}{\Phi})\sqrt{K_r K_c} \tag{10}$$

Once the Φ factor has been calculated, the model can successfully calculate growth rates for both regular and irregular eutectics, provided that the Peclet number, p_c, remains much less than one. The Peclet number is a common measure of interface growth conditions for coupled growth which is defined as

$$p_c = \frac{Vl}{2D} \tag{11}$$

where V is the velocity of the interface, l is the length scale of the microstructure, and D is the diffusion coefficient of solute in liquid. This condition is met in most conventional solidification methods, and is assumed in the JH model. This model assumes both that the eutectic spacing is much smaller than the diffusion distance, and that the interface undercooling is small enough that the interface composition remains about the same as the eutectic composition.

Under rapid solidification conditions, p_c can become larger than one and the two assumptions made by the JH model begin to break down. Recognizing this, Trivedi, Magnin and Kurz (TMK) [19,20] proposed an extension of the classical JH model which maintains that $V\lambda^2$, $\Delta T\lambda$ and $\Delta T^2/V$ are not constants, as assumed by JH, but deviate slightly when p_c becomes very large. The TMK model maintains that the eutectic spacing varies according to

$$V\lambda^2 = a^L / Q^L \tag{12}$$

where a^L is a capillarity constant as defined by JH [15] and

$$Q^L = \left(\frac{C_o}{Df(1-f)}\right)\left[P + \lambda\frac{\partial P}{\partial \lambda}\right] \tag{13}$$

where P is a function of the volume fraction of the α-phase and p_c as described by TMK [19]. Interface undercooling can then be calculated from λ as shown in Eq. 14.

$$\Delta T\lambda = ma^L\left[1 + \frac{P}{P + \lambda(\partial P/\partial\lambda)}\right] \tag{14}$$

Rapid Solidification Studies of Al-Si

Because of the simplicity of the phase diagram (see Figure 6) and the large number of industrial applications, a wide variety of rapid solidification studies have been carried out on the Al-Si system, using a number of different techniques and concentrating on a range of compositions. Several relevant studies are described below.

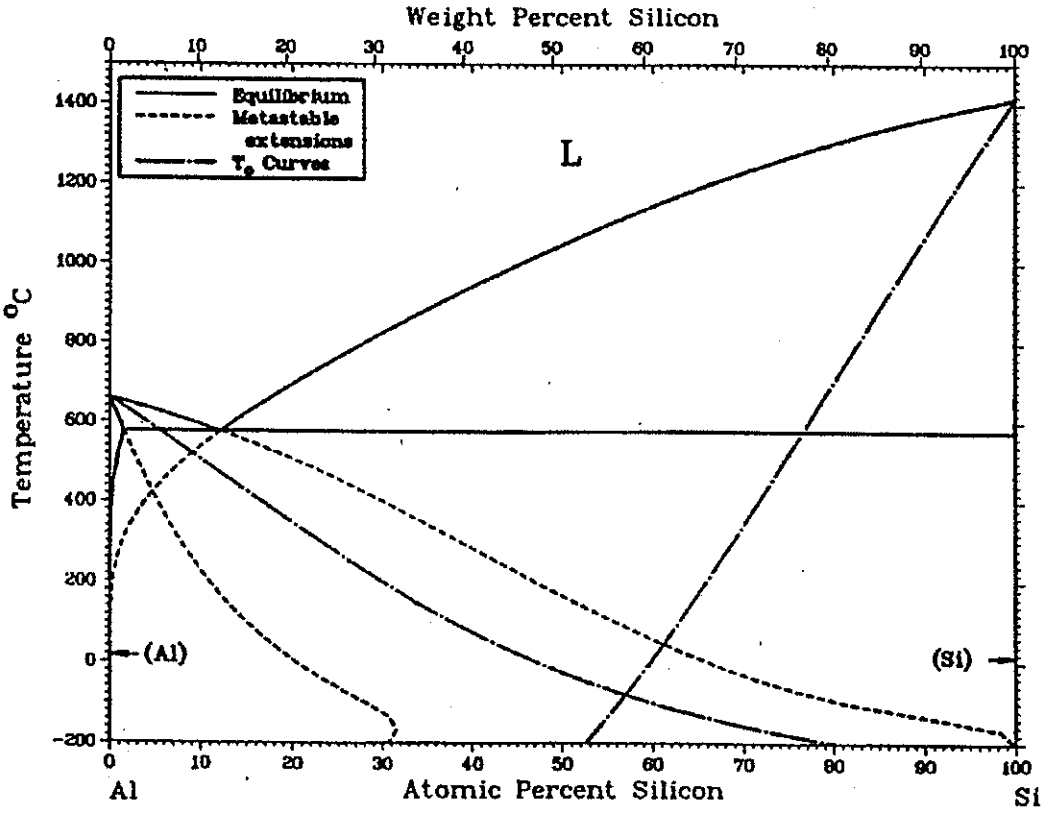

Figure 6. Metastable Al-Si Phase Diagram [21].

Some of the early rapid solidification work on Al-Si was done by Levi and Mehrabian [6], using submicron particles produced by electrohydrodynamic (EHD) atomization. Al-3%Si and Al-6%Si hypoeutectic compositions were studied. Note that throughout this thesis, all compositions are given as weight percent unless otherwise indicated. Using TEM analysis, they found that most particles in the 0.1-1.0 μm range showed a structure with three

distinct regions. First, a supersaturated solid solution formed, which grew with a planar interface and quickly precipitated out very fine Si clusters. As the droplets experienced recalescence, the driving force for solute trapping decreased, causing a segregate-free zone to form and the buildup of Si supersaturation in front of the growing interface. Finally, the interface became unstable and broke into cells. They found that smaller particles were more likely to avoid segregation, which was attributed to an increased undercooling and more rapid solid/liquid interface velocity. A small faction of particles was also observed which showed large faceted silicon crystals. These crystals were more often observed in larger particles with higher Si content.

More recently, microstructural characterization of the Al-Si eutectic composition has been carried out by Birol [22] using melt spinning. At a cooling rate of 10^6 K/s, similar to that experienced by atomized powder, a cellular structure was observed with nanoscale Si particles distributed throughout the cells. In thinner sections of the ribbon, a 'featureless' region was observed in addition to the cellular region, which was attributed to an increased cooling rate.

Wang et al. [23] used the drop tube technique to obtain particles of Al-18Si ranging from 60 to 1000 μm in diameter for microstructural study. They found that in particles larger than 500 μm, polygonal primary Si crystals were present, surrounded by eutectic Si distributed homogenously in an α-Al matrix. In particles smaller than 500 μm, star-shaped primary silicon formed, along with spherical eutectic grains, composed of anomalous eutectic at the core with lamellar eutectic radiating outward. Cooling rates of 3.8×10^5 K/s and 3.9×10^3 K/s were calculated using the Newtonian cooling model for the high and low extremes, respectively.

Al-20Si produced by gas atomization has been studied by Hong and Suryanarayana [8] as well as by Kim et. al. [24]. Kim examined the microstructure using both SEM and TEM techniques, and found that primary silicon crystals of approximately 3 μm formed first in the droplets, followed by metastable eutectic solidification of the remaining liquid into α-

Al and Si. The eutectic Si was measured to be about 100 nm. The interface between the Si and the Al was found to be semicoherently bonded along the Al {111} and Si {111} planes.

Hong and Suryanarayana also report primary Si in an aluminum matrix or eutectic structures. In powders larger than 45 μm, primary silicon very similar to that reported by Kim et. al. is shown; however in particles smaller than 26 μm, the authors were unable to distinguish between primary and eutectic Si due to the fineness of the microstructure and similarity in size and shape between the two phases. Mechanical testing of bars made from extruded powder samples showed that bars made from Al-20Si powder <26 μm in diameter had a significantly higher UTS and significantly decreased wear rate due to sliding than bars made from the same composition with powder 45-106 μm in diameter [8]. The difference in properties was attributed to the difference in microstructure between the two size classes of powder.

Laser surface melting of compositions varying from 15.5 to 20% Si was used by Pierantoni and colleagues [25] to experimentally find the Al-rich boundary of the coupled zone. Their results, which are consistent with a coupled eutectic solidification zone skewed toward the faceted side of the phase diagram, as previously determined [26], are shown in Figure 7. Above 20% Si, primary silicon crystals began to form through nucleation in the liquid. These crystals were surrounded by α-Al cells in a larger eutectic matrix. The study concluded that the mean eutectic spacing was independent of silicon content and affected only by solidification rate, with a minimum eutectic spacing measured at 45 nm.

Trivedi et al. [7] refined this work by developing a more complete map shown in Figure 8, which predicts the growth morphology of an atomized Al-Si particle with respect to composition and undercooling. Note that the map is only concerned with growth, and that in a real system, nucleation effects will also impact the final microstructure. This map was produced from the study of the eutectic composition (12.6 wt% Si). The current study uses hypereutectic compositions in an attempt to verify the map and to explore further the microstructure selection in hypereutectic alloys, using gas atomization to promote a deeply undercooled condition.

The results predicted by this map have been observed in rapidly solidified powder in related systems. Mueller and colleagues [27] found that in gas atomized Al-4at%Be powders cooled at 500°C/s, primary Be formation was avoided and solidification commenced with a cellular aluminum and intercellular beryllium structure. The cells evolved into a dendritic network during recalescence, which was replaced by a coupled eutectic morphology following recalescence. Bendersky and colleagues [28] studied Al-5Mn-5Fe-2Si powder and found that droplets less than 20 μm were capable of cooling below the lower boundary of the skewed coupled zone and nucleating aluminum. Crystallization started with microcellular Al with an amorphous or very fine polycrystalline phase as an intercellular constituent. Recalescence produced either an extreme change in cell dimension or the formation of a eutectic.

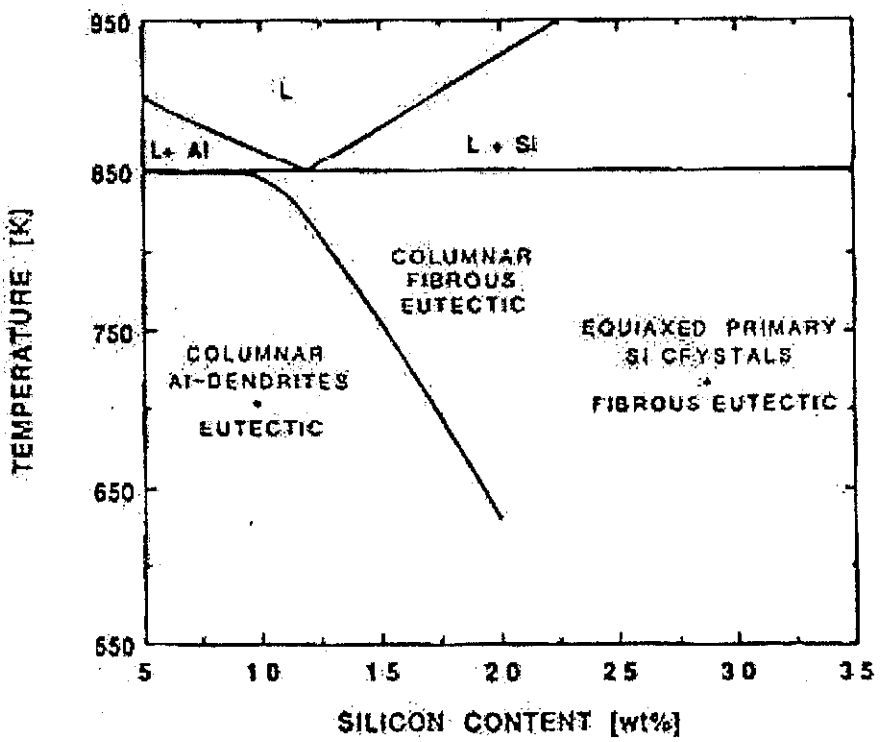

Figure 7. Calculated Al-rich limit of the coupled zone.

According to the map, it should be possible to produce particles with uniform coupled growth. The fine microstructural spacing resulting from coupled growth in deeply undercooled droplets will provide improved mechanical properties, according to the Hall-Petch relationship. If atomization could be utilized to produce powder with a uniformly fine two-phase microstructure, a material with exceptional strength and toughness would result. Such an ideal microstructure, if maintained in a fully consolidated part, presents many exciting possibilities for industrial applications.

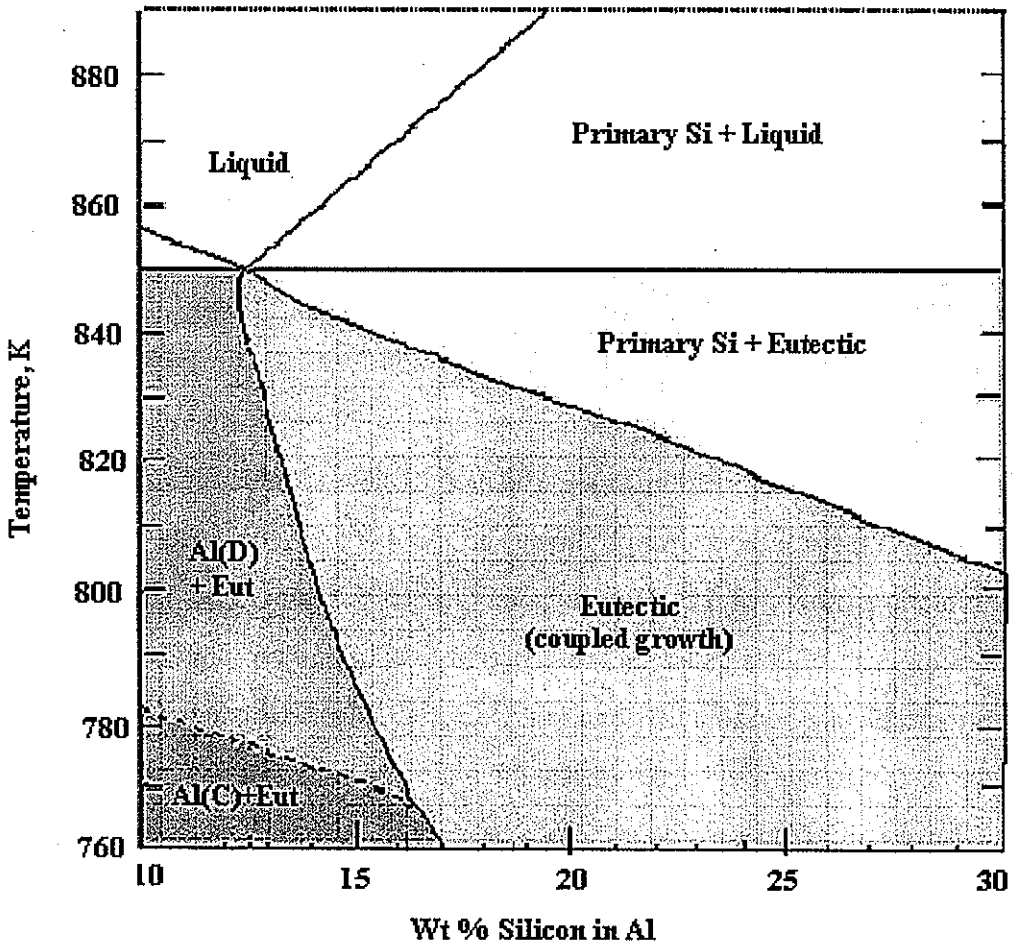

Figure 8. Growth morphology map for the Al-Si system.

EXPERIMENTAL PROCEDURE

Gas Atomization

The atomizer, shown schematically Figure 9, consists of three main parts: the melt chamber, the spray chamber, and the powder collection system. The melt chamber was charged with high purity (99.95%) Al and Si in lump form for each experiment to a total weight of about 1.5 kg. Each charge was induction melted in a hard-fired, high purity (99.7%) Al_2O_3 bottom pouring crucible, which was sealed by a similar Al_2O_3 stopper rod. Based on liquidus temperatures of about 620°C and 680°C, pouring temperatures of 1100°C and 1300°C were used for atomizing the Al-15Si and Al-18Si alloys, respectively.

A plasma arc spray-deposited ZrO_2 pour tube with a melt orifice diameter of 1.7 mm served to guide the melt to the HPGA nozzle. This nozzle, illustrated in the inset of Figure 9 and again in Figure 10 had a 45° apex angle and 30 cylindrical jets, each with a diameter of 0.74 mm, equally spaced around the melt feed tube tip. When the melt stream enters the wake area of the high velocity gas flow at the melt feed tube tip, the melt immediately forms a complete or partial film flowing radially outward. No extension of the cylindrical stream is projected into the atomization zone. The melt behavior in this region is influenced both by a local low pressure zone which forms at the base of the melt tube, and by a strong recirculation flow which runs counter to the stream flow direction [29]. These complimentary effects cause the melt stream to split and fan outward and the resulting melt film to accelerate horizontally toward the external edge of the feel tube. A significant portion of the melt disintegration occurs when the melt film makes initial contact with the supersonic gas flow at the feed tube edge. Because of this, using a faster, lower viscosity gas (He) increases the sheering force on the melt film and results in a finer droplet distribution.

For one run of each alloy, N_2 (ultrahigh purity grade, 99.995%) atomization gas was used with a supply pressure of 6.6 MPa. For the other run, He (ultrahigh purity grade, 99.995%) atomization gas, with a significantly higher heat transfer coefficient [12], was used

with a supply pressure of 5.5 MPa. After breakup, solidification of the droplets occurred as they fell downward through the spray chamber. He gas was also added into the spray at a downstream location during freefall of the particles in all cases to promote additional convective cooling of the particles.

A cyclone separator was incorporated into the system to collect the particles while allowing the atomization process gas to escape and be vented out of the system.

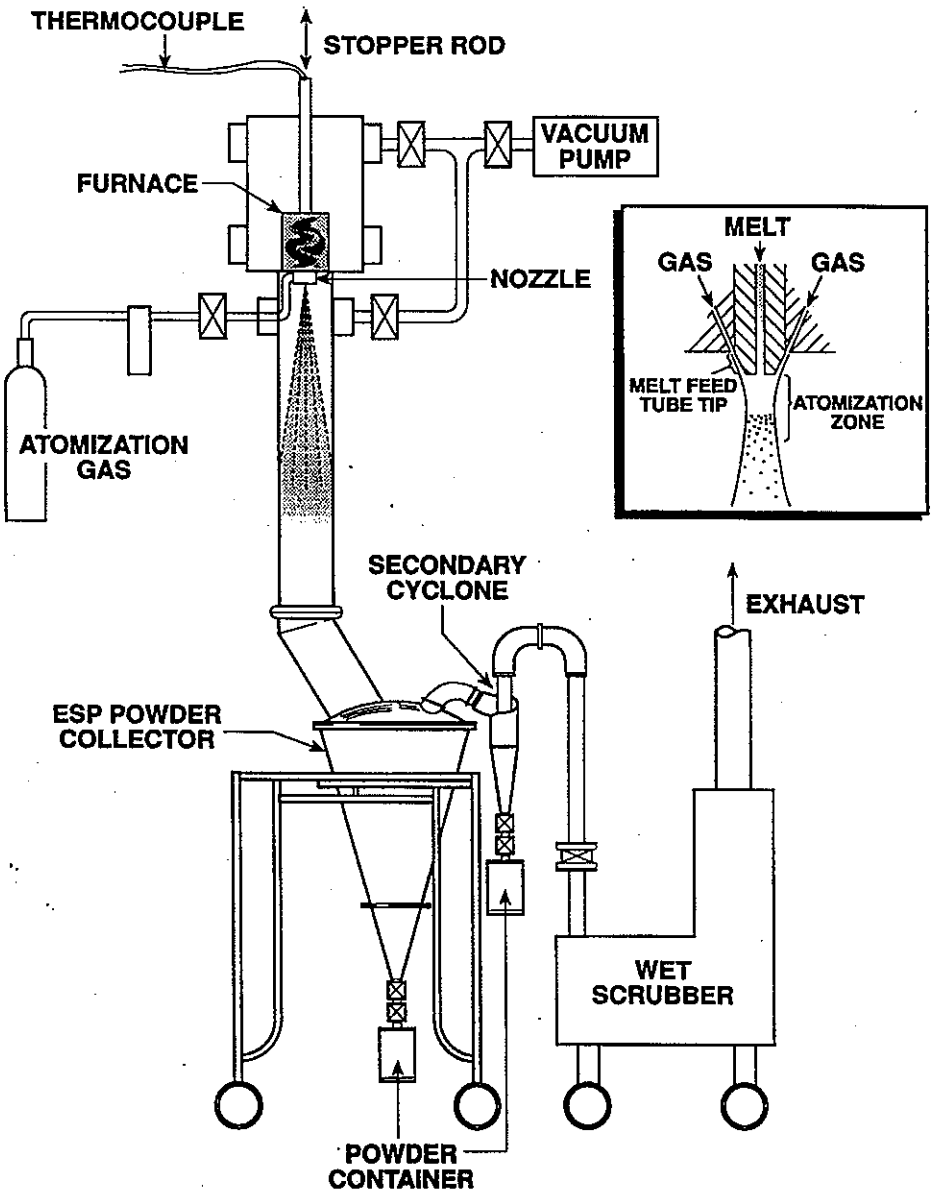

Figure 9. Vertical gas atomizer.

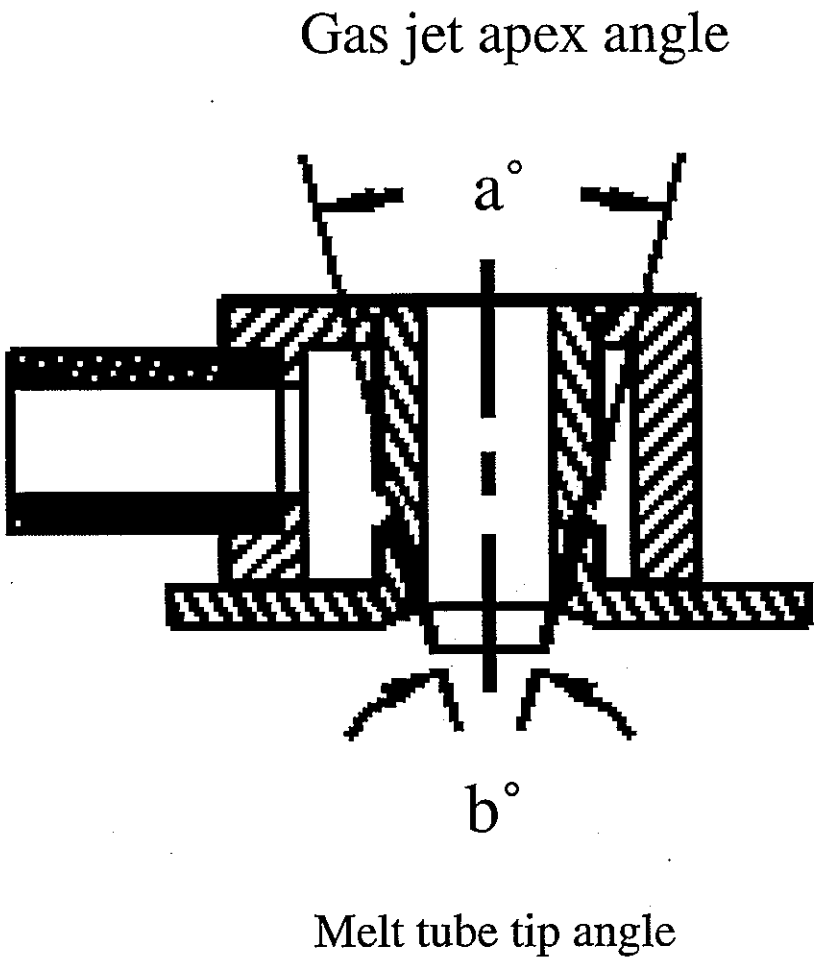

Figure 10. Diagram of nozzle used in atomizer where a = b = 45° for the 30 cylindrical discrete jets in the circular array.

Sample Preparation

The powder collected from both experiments was screened using an ASTM standard sieve with a vibratory shaker to obtain particles of 45 μm in diameter or less. The powder was etched with an aluminum bright dip composed of 44 ml phosphoric acid, 16 ml water and 2 ml nitric acid. The etched loose powder, deposited on conductive carbon tape, was observed with SEM and size ranges corresponding to different microstructures were determined. Those ranges were used to determine subsequent size cuts, and the powder was screened into the selected size classes. ASTM standard screens of sizes 45, 38, 32, 25, and 20 μm were used on the Al-15Si powder, while 45, 32 and 20 μm were used on the Al-18Si powder. Air classification was used to obtain 5-10 μm and <5 μm diameter powder.

After screening, each size class was vacuum dehydrated at ambient temperature and mounted in Epoxicure, obtained from Buehler Ltd., Lake Bluff, Illinois. Five parts resin were mixed with one part hardener for five minutes. To insure regions of high powder density in the resin, a small amount of epoxy was mixed with a large amount of powder on the detachable bottom of a mounting cup. A paperclip was used for this mixing. The cup was then reassembled, and placed in a vacuum chamber with the remaining epoxy. After the majority of bubbles were pulled from the epoxy, it was poured into the cups while still under vacuum. The filled mounts were removed from the vacuum chamber and allowed to dry overnight.

The samples were ground with 600 grit SiC paper and water for two minutes and hand polished with aqueous slurries of 0.3 μm alumina and 0.05 μm alumina. A Master solution of colloidal silica was used on an automatic polisher for two hours as a final step. Each polished mount was then etched with Keller's reagent (2.5 ml nitric acid, 1.5 ml hydrochloric acid, 1 ml hydrofluoric acid, 95 ml water) for approximately 8 seconds. To facilitate electron microscopy, the mounts were painted around the sides with carbon paint and sputter coated with gold at 6 volts for two minutes.

To screen additional alloys richer in Si for future gas atomization experiments, six other compositions between Al-25Si and Al-35Si were produced and converted to melt-spun ribbon. A melt spinner with a water cooled copper wheel was used at a wheel speed of 22 m/s. The ribbons were analyzed using x-ray diffraction to search for any potential glass forming compositions. Ribbon samples were also mounted in epoxy, polished, etched and observed in cross section with an optical microscope to confirm diffraction results.

Microstructural Analysis of Powder

The mounted powder was observed in cross section using a JOEL 6100 scanning electron microscope, which has a resolution limit of about 20 Å. An accelerating voltage of 20 kV was used, along with a working distance between 15 and 10 mm and a spot size ranging from 23 to 30. The SEM was operated under high vacuum conditions up to a magnification of 35,000X.

All images of the powder were recorded digitally. Quartz PCI version 5.1, an image analysis software package, was used to measure particle sizes and microstructural spacings.

EXPERIMENTAL RESULTS

Deep Etching of Loose Powder

The results of the deep etching showed good initial correspondence with the predictions of the map in Figure 8. Distinctly different microstructures were observed in the Al-18Si powder corresponding to the undercooled regions which the 15% line passes through on the map. Below a diameter of 10 μm, a two phase structure was observed that appeared to be microcellular aluminum, as shown in Figure 11. The majority of larger particles observed appeared to have nucleated single crystals of silicon, which are easily recognizable by their hexagonal shape and because they are raised above the surface of the particles which have been etched to remove aluminum. These crystals are apparent in both Figure 12 and Figure 13. Particles with nucleated silicon were observed in some fraction of particles at all diameters greater than 10 μm and constituted the largest total fraction of particles. No Si dendrites were observed at any size fraction.

In most particles, aluminum cells or dendrites heterogeneously nucleated on the surface of the Si crystals from the silicon-depleted liquid. The aluminum dendrites grew until they were overtaken by eutectic growth. This is exemplified in Figure 12. The growth of these dendrites varies widely, and in some cases they are missing entirely, with the coupled growth beginning directly next to the silicon crystals. An example of such a particle is shown in Figure 13. In some particles between 10 and 37 μm in diameter, aluminum dendrites that did not nucleate from silicon crystals were observed, as shown in Figure 14. The Si-nucleated Al dendrites are easily distinguishable from those which nucleated without Si catalysts because of the increased directionality of their growth, apparently caused by the faceted sides of the silicon crystals, acting as epitaxial nucleant surfaces.

At the composition Al-18Si, two types of particles were observed. Most of the particles showed primary silicon crystals surrounded by aluminum dendrites and coupled eutectic. No silicon dendrites were observed at any size fraction. In particles with diameters

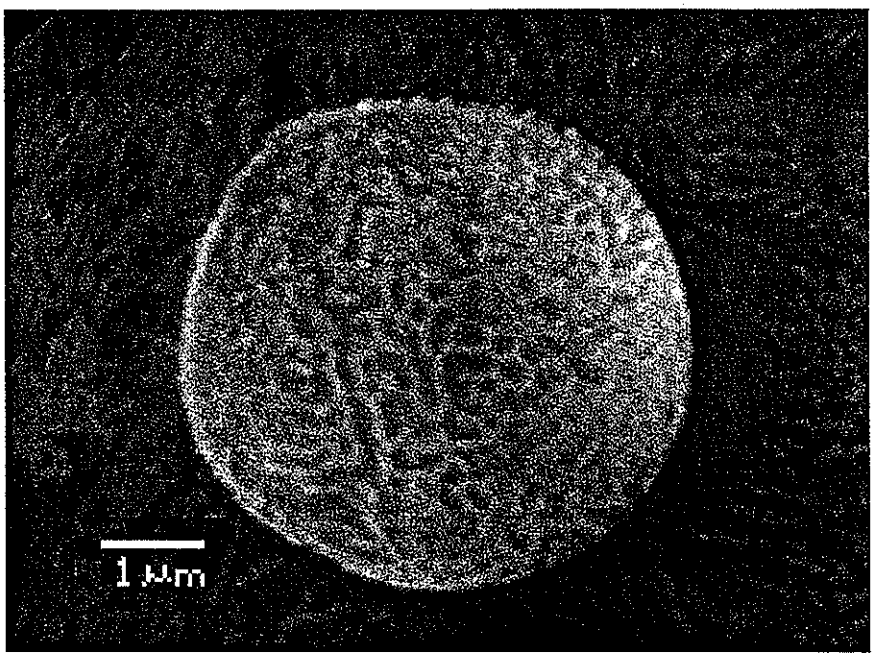

Figure 11. 5 µm particle, Al-15 Si, N_2 atomized. 10,000X

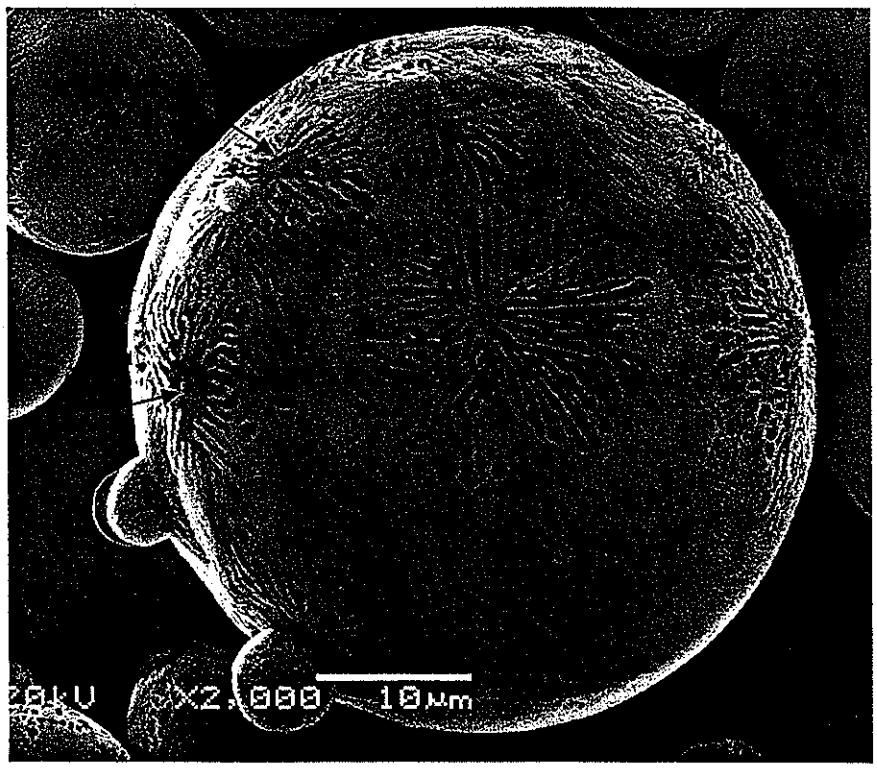

Figure 12. Eutectic surrounding Si-nucleated Al dendrites.
The boundaries between the eutectic colonies are clearly visible.
Selected Si crystals are indicated by arrows.
45 µm particle, Al-15Si, N_2 atomized. 2,000X

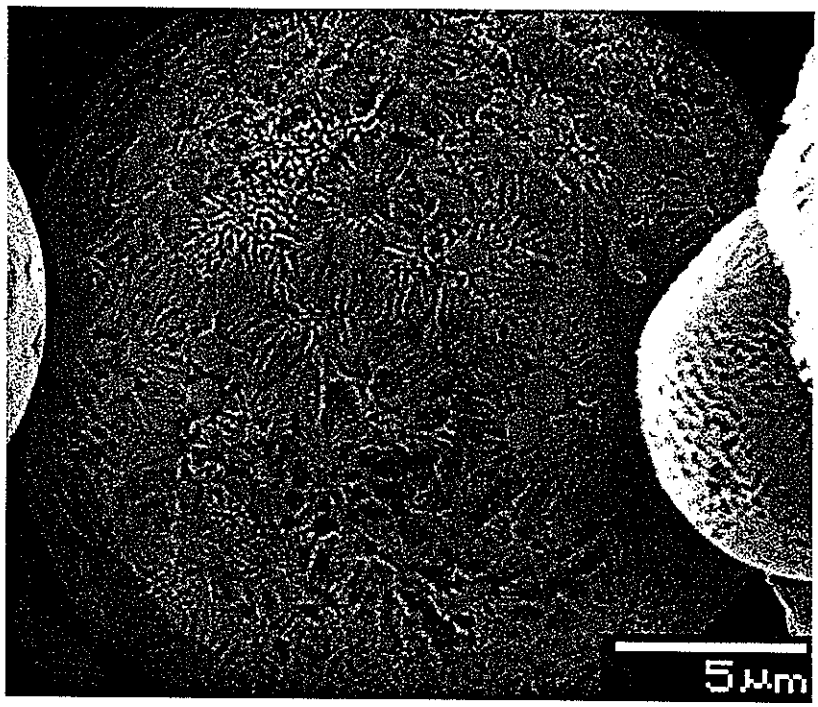

Figure 13. Coupled eutectic with primary Si crystals which clearly display a hexagonal shape.
22 µm particle, Al-15Si, N_2 atomized. 3,500X.

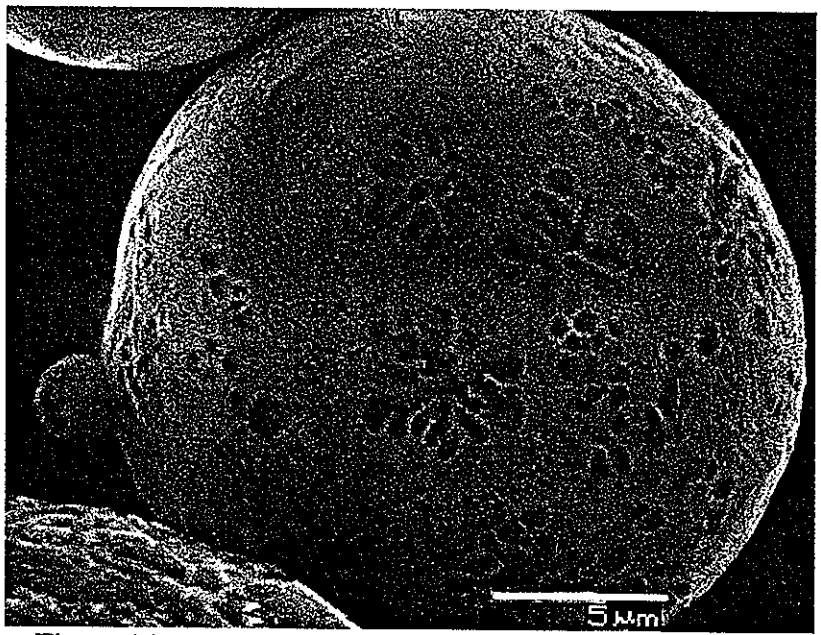

Figure 14. Al dendrites which formed without Si nucleant. The Al-rich phase has been etched away.
21 µm particle, Al-15Si, N_2 atomized. 4,500X

between 5 and 10 μm, there was generally a single nucleation site for the dendrites, while the larger particles had multiple nucleation sites and many dendrites. This method was not successful for observing particles below ~5 μm. An example of a very small particle with a single nucleation site can be seen in Figure 15. The three slightly smaller particles show a barely resolvable eutectic structure, while the smallest particles show no resolvable structure at this magnification. The image also shows the prevalence of extremely fine (<1μm) satellite particles which are much more prevalent in the helium atomized powders. As expected, the average size of the powder atomized with He is significantly smaller than the powder atomized with nitrogen [3]. Like the previous composition, some of the particles showed crystals of silicon with coupled eutectic growth and no dendrites.

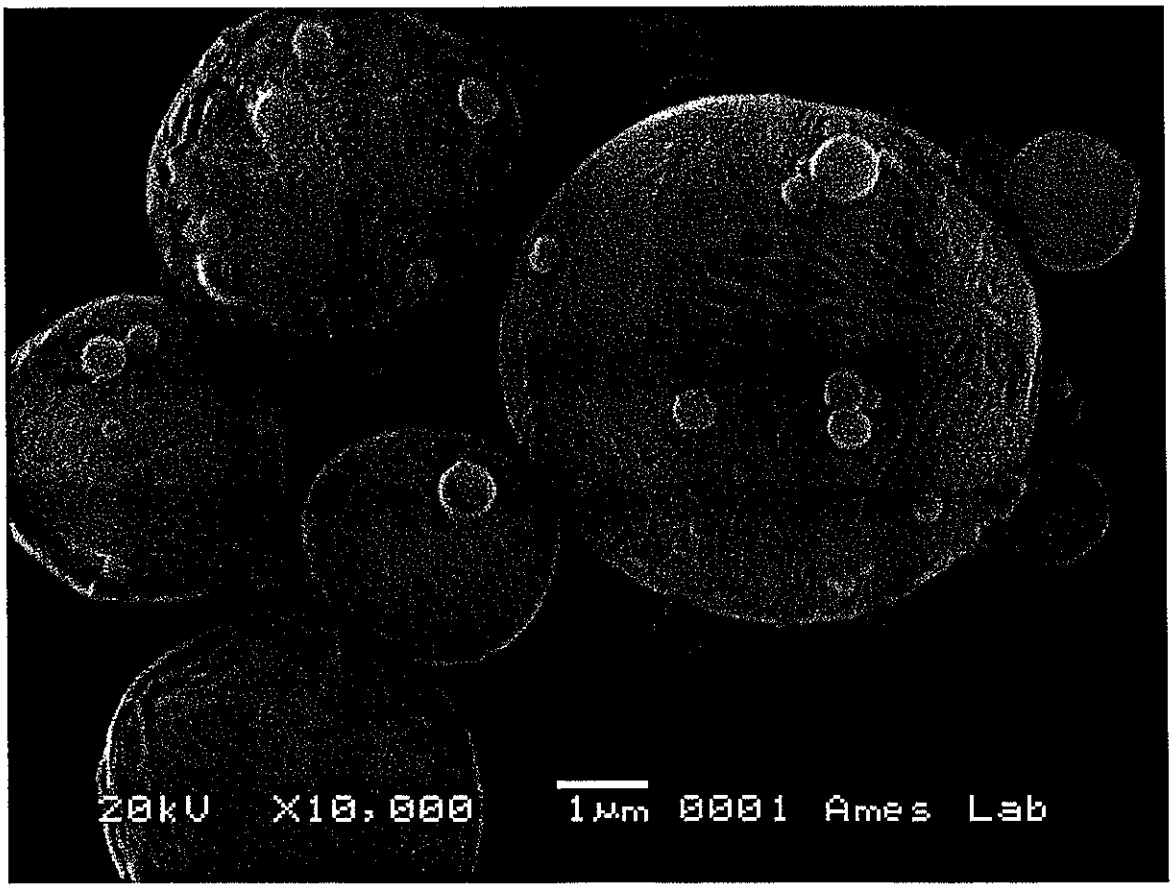

Figure 15. Single crystal particle with nucleation site clearly visible.
≤6 μm particles, Al-18Si, He atomized. 10,000X

It should be noted that the particles shown here were chosen because they clearly showed the microstructures being described. The competing effects of nucleation and growth and the competition between different morphologies, along with the added effects due to atomization, such as collisions between droplets or collisions of droplets with the atomizer walls, make it difficult to definitively classify the microstructures observed in many of the particles.

Microstructure Observations from Cross Sectioned Powder

After initial work with the deep-etched powder, the cross-sectioned powders were used to perform a systematic study of the relationship between microstructure and undercooling. For a given gas, it was assumed that the diameter of the particle is directly related to undercooling, so particles are classified here by diameter. The largest nitrogen atomized particles of Al-15Si, those greater than 40 microns in diameter, show a large number of the primary silicon crystals surrounded by aluminum-rich areas which may take the form of small cells or dendrites. These regions are quickly overtaken by a highly irregular coupled eutectic structure (Figure 16). As particle size decreases, the number of silicon crystals decreases. As the particle size decreases below 30 μm, the aluminum dendrites become larger and more branched. Below 20 μm, no primary silicon was observed, and the aluminum dendrites, surrounded by eutectic, reached across the entire diameter of the particle (Figure 17). As the diameter decreased farther, the average number of nucleation sites decreased to three or less. Particles down to 5 μm were studied at this composition.

Particles of the same composition atomized with helium showed a much more uniform morphology across all particle sizes studied. Virtually all particles showed small aluminum dendrites surrounded by a very fine coupled eutectic which comprised a large fraction of the volume of the particle (Figure 18). Silicon crystals were only occasionally observed. A few particles showed larger Al dendrites which reached across the diameter of the particle. Particles down to 1.5 μm were studied at this composition.

Two morphologies were observed in the Al-18Si particles which were atomized with He. The largest particles of 18%Si were similar to the largest 15%Si particles, with Al-rich regions and a coupled eutectic phase surrounding faceted Si crystals. Smaller particles were more likely to show larger, more complex, oriented Al dendrites apparently nucleating from Si crystals and surrounded by a large fraction of eutectic (Figure 19). Comparing Figures 18 and 19 will provide a view of the difference between the aluminum dendrites found in 15%Si particles and those present in 18%Si particles. Coupled eutectic of an extremely fine scale was present in a number of these particles (see Figure 20). It is very similar in appearance to the 'anomalous' eutectic reported by Wang [23]. Powders down to 2.5 μm were studied at this composition.

Only a preliminary study of the Al-18Si powder atomized with N_2 has been carried out so far, but it appears that these particles have structures generally similar to the 18% powder atomized with He. There are, however, a larger number of primary Si nucleation sites, and the spacing of the eutectic noticeably coarser. An example of a typical particle is shown in Figure 21. The presence of large, oriented Al dendrites is also reduced, with only a few instances of that morphology observed in the smallest particles. Powders down to 8 μm were studied at this composition.

The most thorough study of the smallest particles was made on the Al-15Si He atomized powder. It was discovered that below a diameter of approximately 4 μm, the interdendritic region changed from a coupled eutectic to an apparent single (Si) phase. Figure 22 shows two very small particles, one representative of those particles observed without a coupled phase, and the other a comparably sized particle at the same magnification which does show a coupled eutectic phase. The single phase may be due to coarsening of an extremely fine coupled structure as described by Lemaignan [30]. If this is the case, the interdendritic region is actually a two phase region, with an extremely fine Al phase distributed through the silicon. TEM work is required to determine if the interdendritic phase is not pure silicon, indicating coarsening since Al has no solubility in Si (refer to phase diagram in Figure 6).

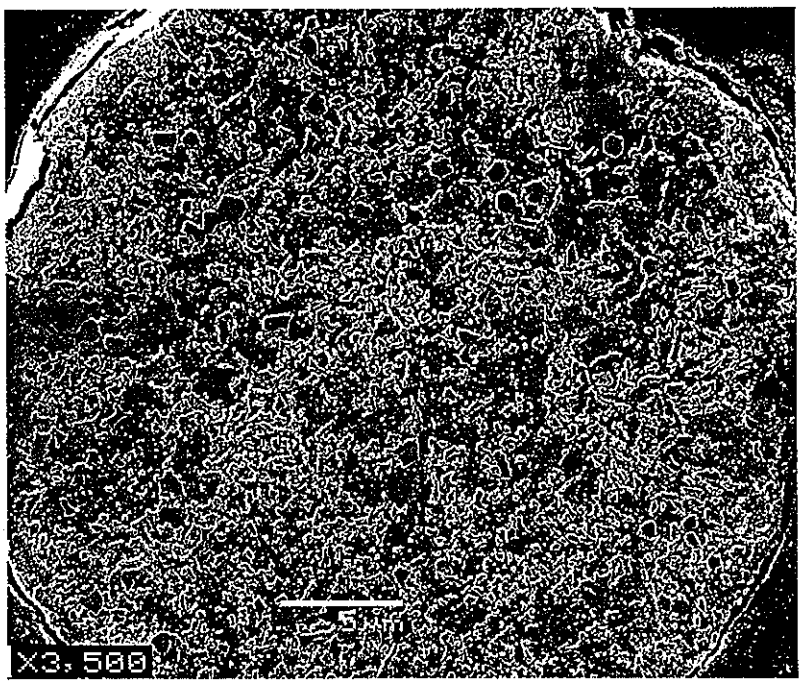

Figure 16. Primary Si + Eutectic;
35 μm diameter, Al-15Si, N_2 atomized. 3,500X

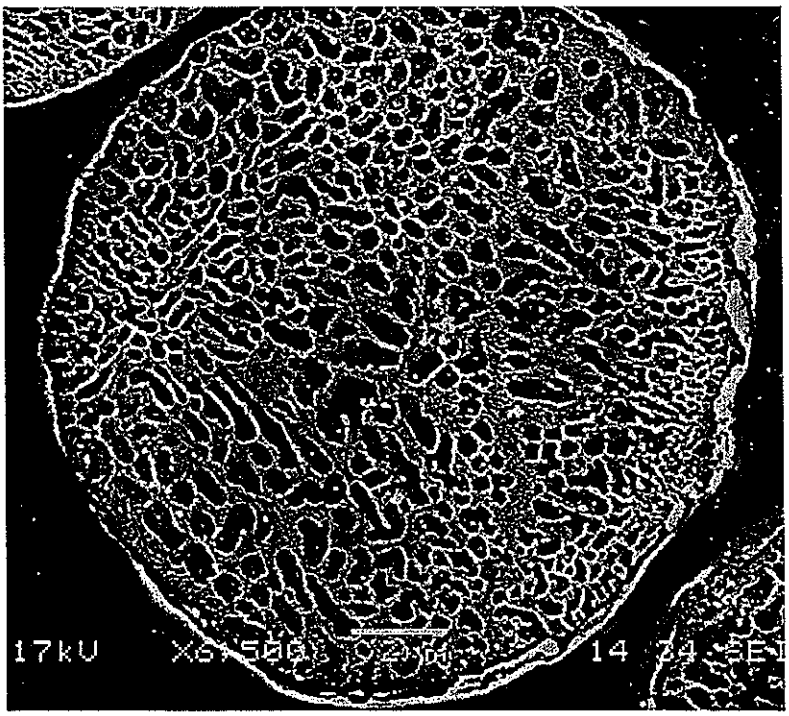

Figure 17. Al dendrites reaching across particle;
15 μm diameter, Al-15Si, N_2 atomized. 6,500X

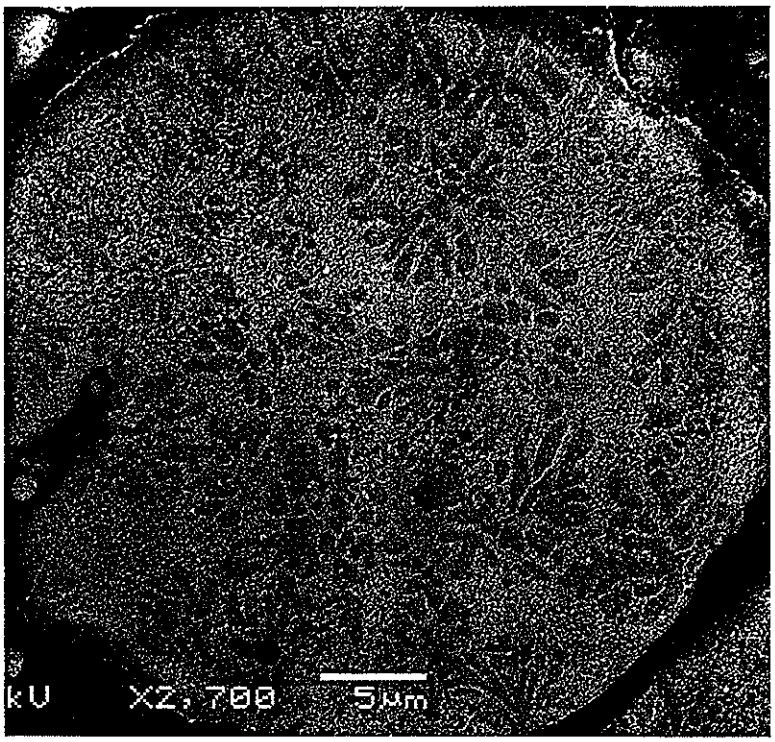

Figure 18. Small Al dendrites + eutectic, no primary Si;
38 µm diameter, Al-15Si, He atomized. 2700X

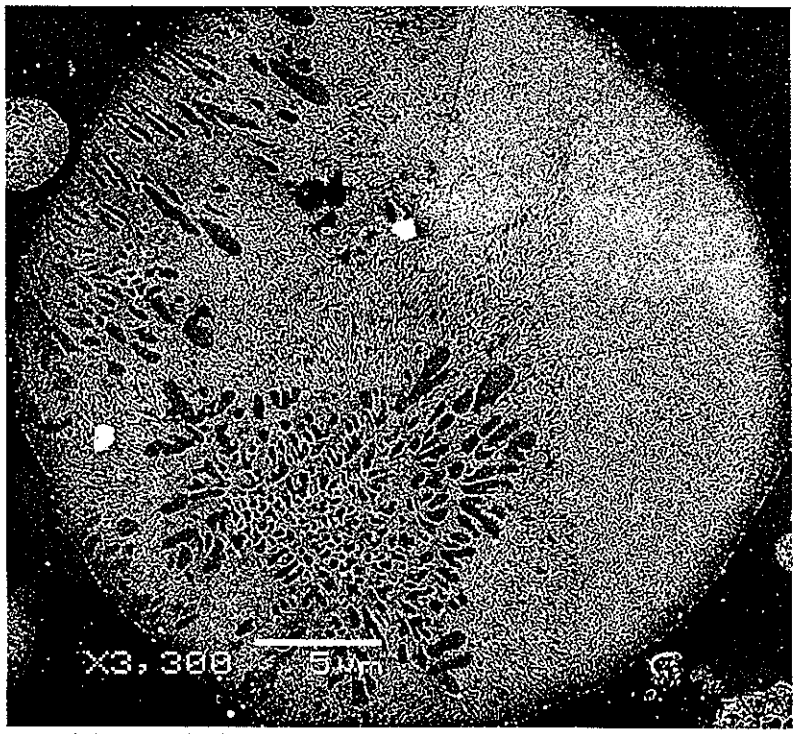

Figure 19. Highly oriented Al dendrites + eutectic;
30 µm diameter, Al-18Si, He atomized. 3300X

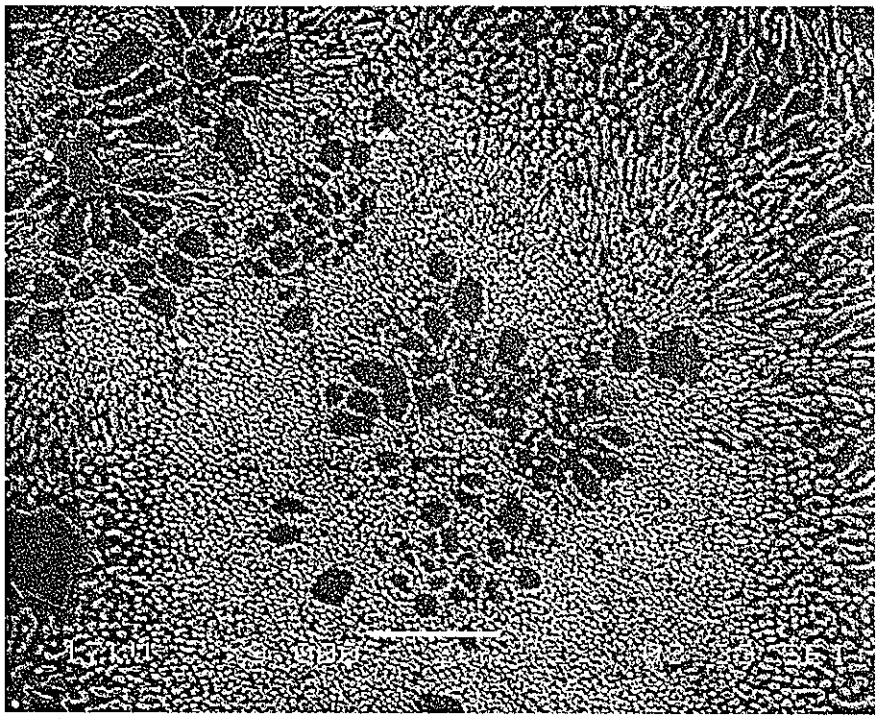

Figure 20. Extreme fineness of coupled eutectic in Al-18Si;
34 μm diameter, Al-18Si, He atomized. 9000X

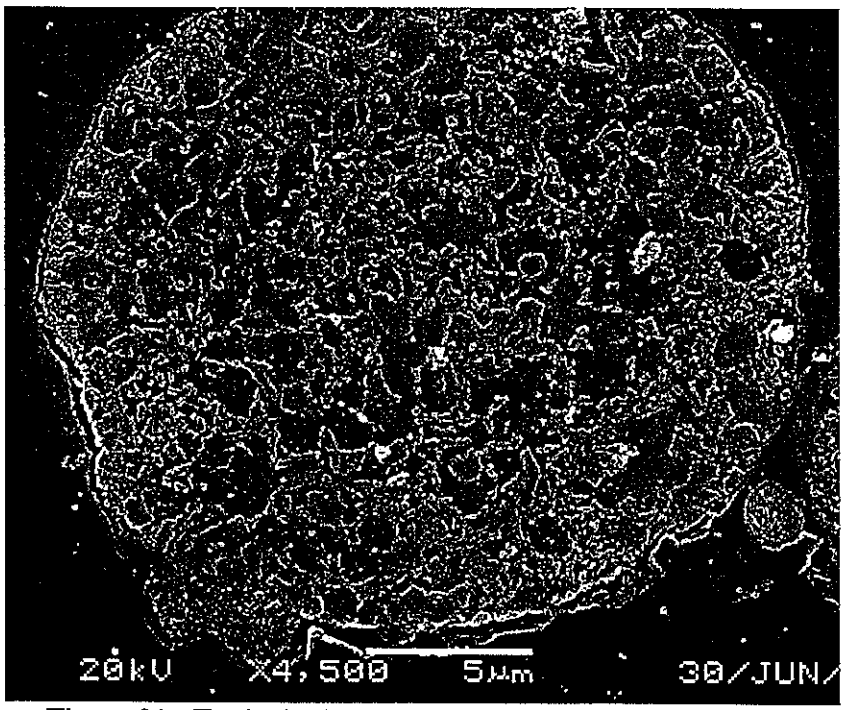

Figure 21. Typical microstructure of N_2 atomized Al-18Si;
22 μm diameter, Al-18Si, N_2 atomized. 4500X

(a)

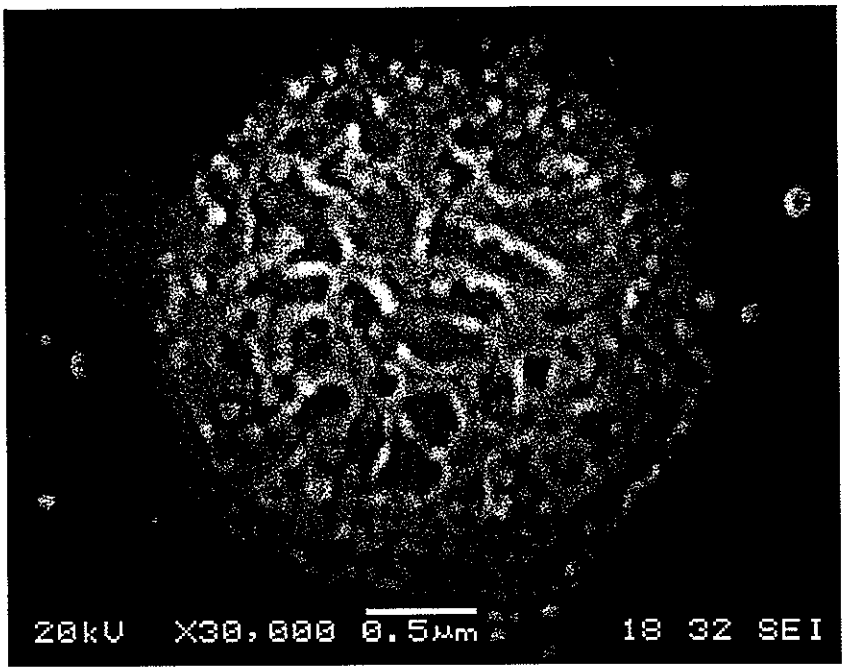

(b)

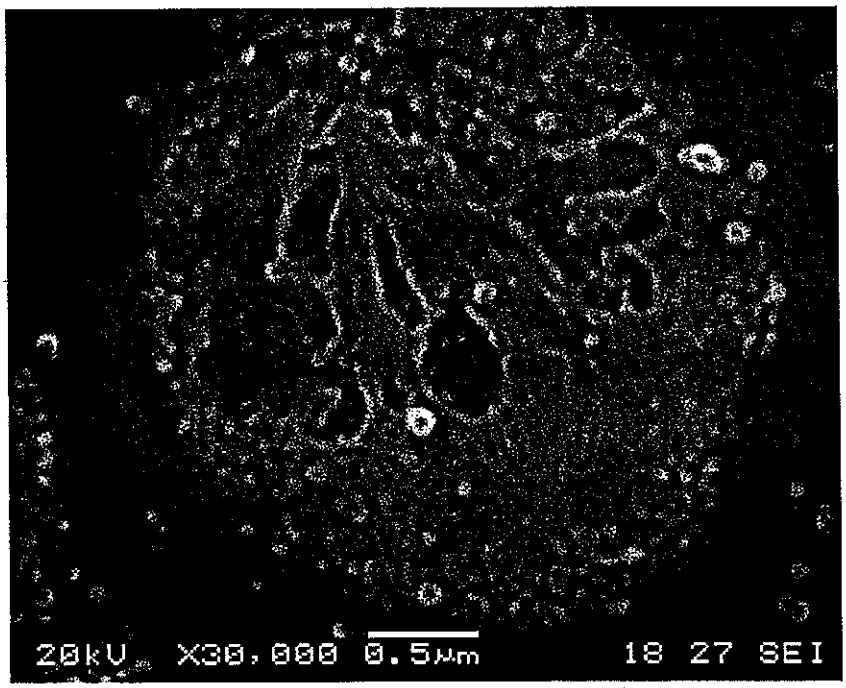

Figure 22. Extremely fine particles showing (a) single phase and (b) coupled eutectic phase surrounding Al dendrites. 2.3 and 3 µm diameter, Al-15Si, He atomized. 30,000X

Atomizer Effects

Atomization is a real metal processing technique, not a carefully controlled experimental technique, and consequently, there are a number of variables affecting the final morphology of the powder which cannot be controlled or, always, identified. The most frequent such effect is the collision of a small solid droplet with a larger liquid or partially liquid droplet, causing a solid phase to nucleate on the surface of the inclusion. This phenomenon was identified in previous work [31], and labeled as "second start nucleation" as opposed to "self start nucleation" when no inclusions are present to cause solidification. That study identified second start nucleation in about 30% of powders. In the larger particles observed in this study, as many as three small inclusions were observed in a single cross section. More would likely become visible if serial sectioning were carried out on the particles. The smallest particle in which an inclusion was observed was 3.5 μm in diameter, with an inclusion of 0.6 μm. Often, in particles containing inclusions which have clearly caused solidification, primary silicon crystals are also present, indicating both types of nucleation were active. Collisions between droplets and chamber walls are another possible cause of morphology variation, but occur in a much smaller fraction of powders.

Figure 23 shows two examples of powders with inclusions. Internal and external inclusions are both present. Note that in the lower Si content composition, Al dendrites nucleate and grow off the surface of the inclusion, while at a higher Si content, eutectic nucleates directly. This is an observable trend, although examples of Al-18Si inclusions nucleating Al dendrites were also noted.

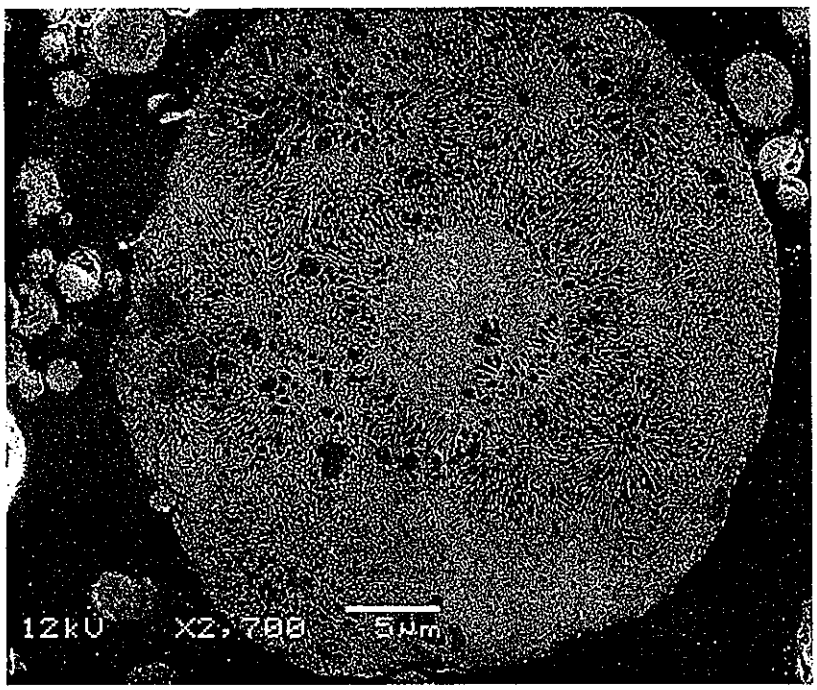

38 µm diameter, Al-18Si, He atomized. 2,700X

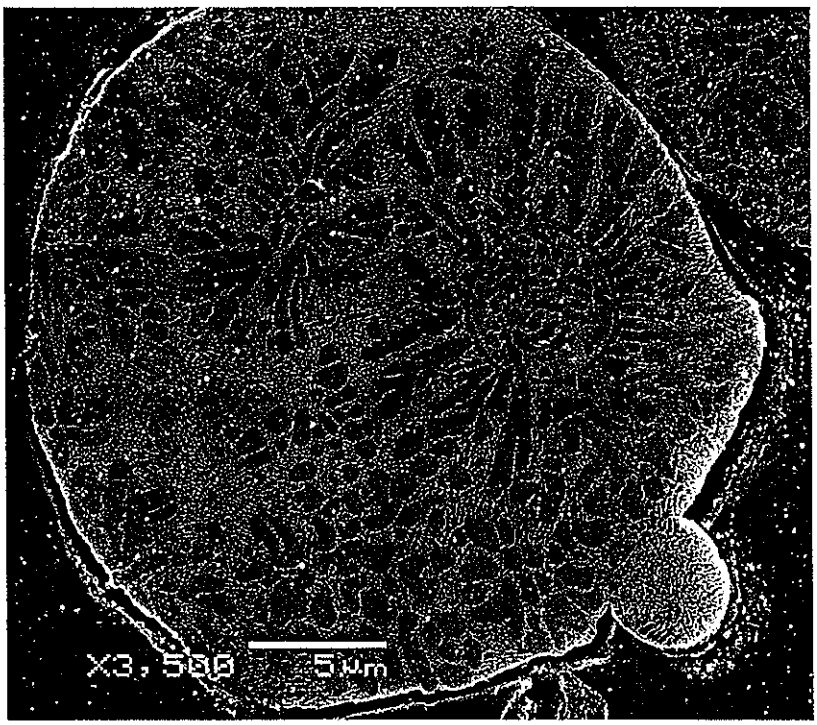

25 µm diameter, Al-15Si, N_2 atomized. 3,500X

Figure 23. Two examples of powder particles containing inclusions and exhibiting "second start nucleation."

Eutectic Spacing across a Range of Powder Sizes

The cross sectioned mounts were also used to measure the change in average eutectic spacing as a function of particle diameter. Using SEM images, the coupled eutectic spacing was measured several times on twenty-five or more particles of varying diameters for each composition. Average spacing was determined for each particle, then spacing was averaged over a small range of particle sizes. The results of the averaged ranges are shown in Figure 24. Maximum and minimum spacings for each range are also included on the graph. Both composition and atomization gas have an effect on average eutectic spacing in the particles. Increasing silicon content causes an increase in eutectic spacing, as does the use of N_2 as the atomization gas. However, no effect from either source is seen in droplets below 11 μm. These trends are confirmed by the results from all four powder samples.

Note that to obtain accurate data points for these graphs, it is necessary to know with some precision the true diameter of the particles on which the spacing measurements are made. The best way to be assured of the true diameter is to use particles which are touching similar sized particles on either side. The powder samples atomized with helium contained very few of the larger size fraction of particles, and so it was not possible to be as selective with the particles chosen for measurement. Some of the powder diameters may have been underestimated, therefore introducing error into the graphs. This difficulty could cause some of the points on the following graphs to be too high.

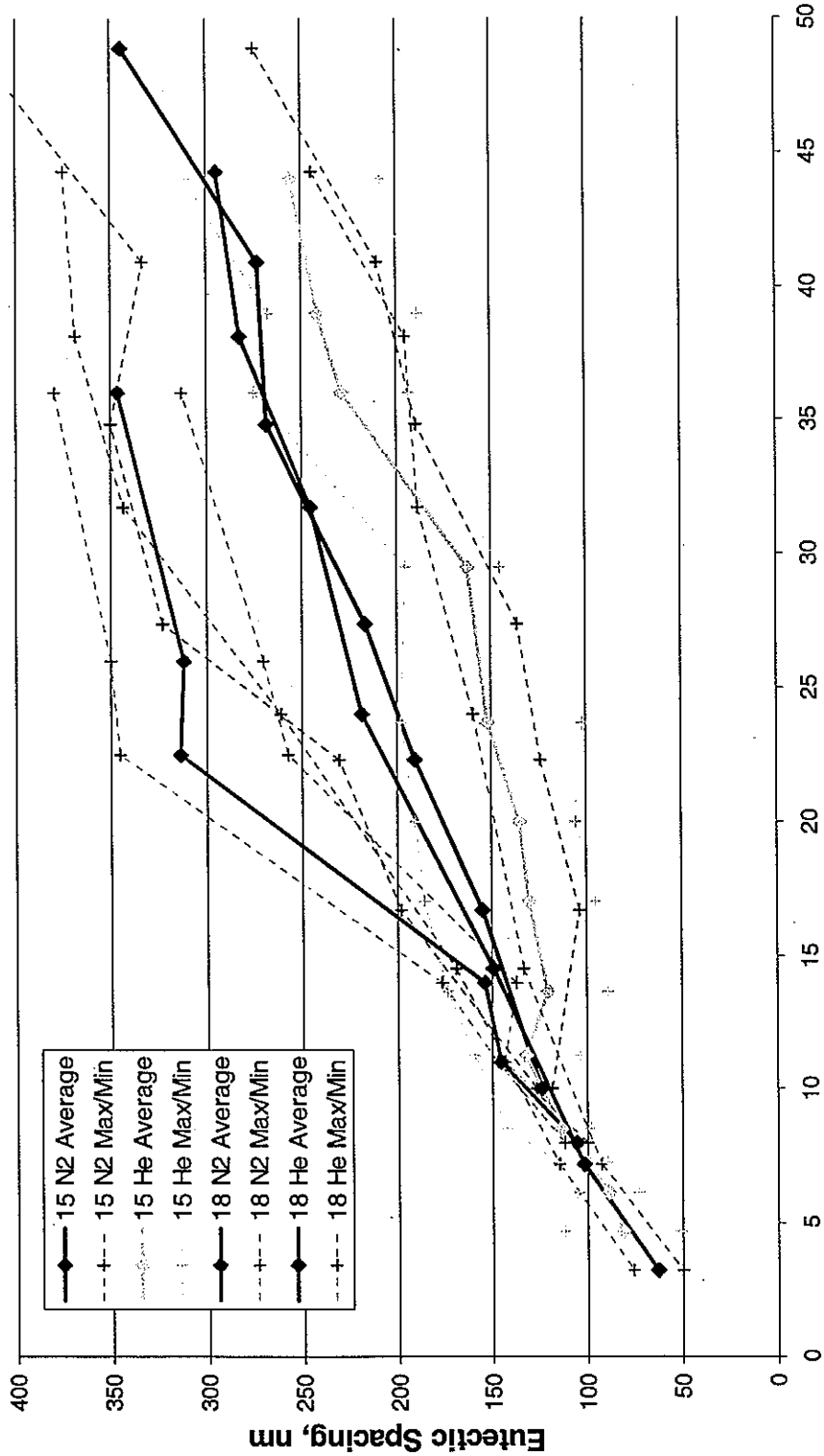

Figure 24. The variation in eutectic spacing as a function of droplet diameter.

Eutectic Spacing in a Single Crystal Particle

While it is useful to understand the correlation between average spacing and particle size, it is necessary to know the exact spacing at the nucleation site to be able to calculate the maximum undercooling reached by a particle. From an apparent single crystal particle in which the nucleation site is visible, measurements of eutectic spacing as a function of distance across the particle were also carried out. An image of the particle is shown in Figure 25, and the results of the spacing measurements are given in Figure 26. Note that the eutectic spacing trend is reversed at large distances, greater than about 37 μm, due to the enhanced local cooling effect from the particle surface.

There is a microstructural transition which occurs partway along the solidification path of the particle. It is shown in close-up in Figure 27. The change is visible in the micrograph as a transition from a highly oriented lamellar eutectic structure (greater than 90% planar orientation) which originates between the dendrites to a more random coupled structure with less than 10% orientation dependence, as determined by line intercept analysis [32]. The same transition from a highly aligned to an unaligned structure is seen in a number of other polycrystalline particles with similar dendrites and spacings, always occurring just beyond the dendrite tips.

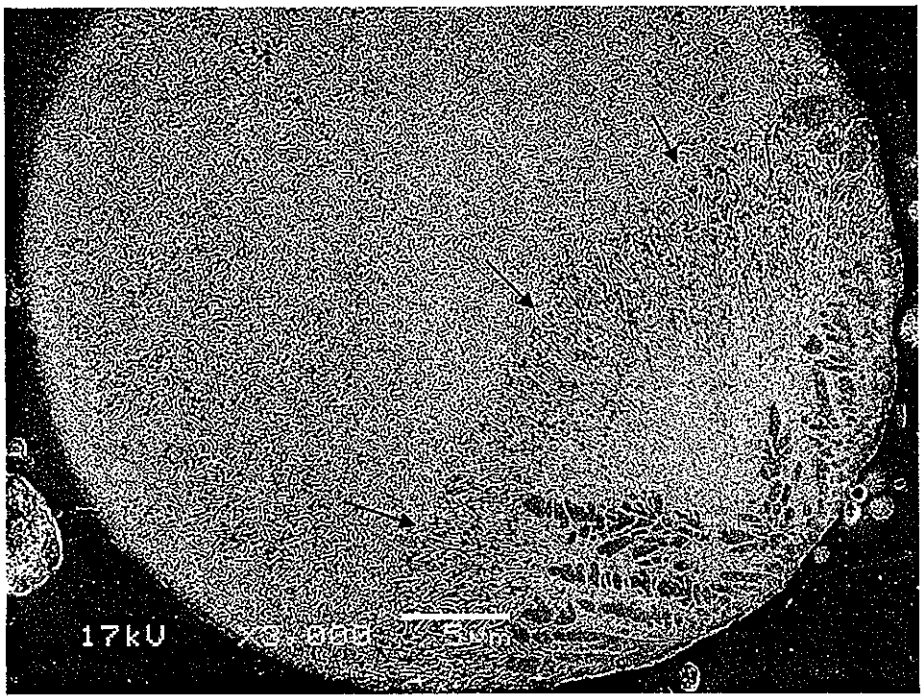

Figure 25. Apparent single crystal particle where the nucleation site is clearly visible. Arrows indicate microstructural transition.
42 μm diameter, Al-18Si, He atomized. 3,000X

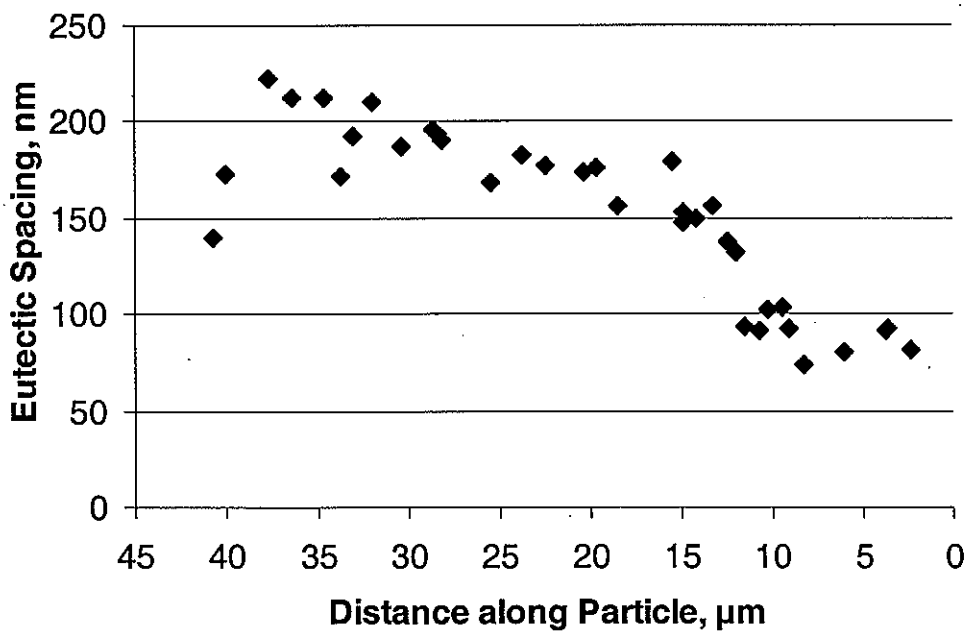

Figure 26. Experimental measurements of eutectic spacing variation with distance within the particle shown in Figure 25. The x axis runs from right to left to match the solidification path of the particle.

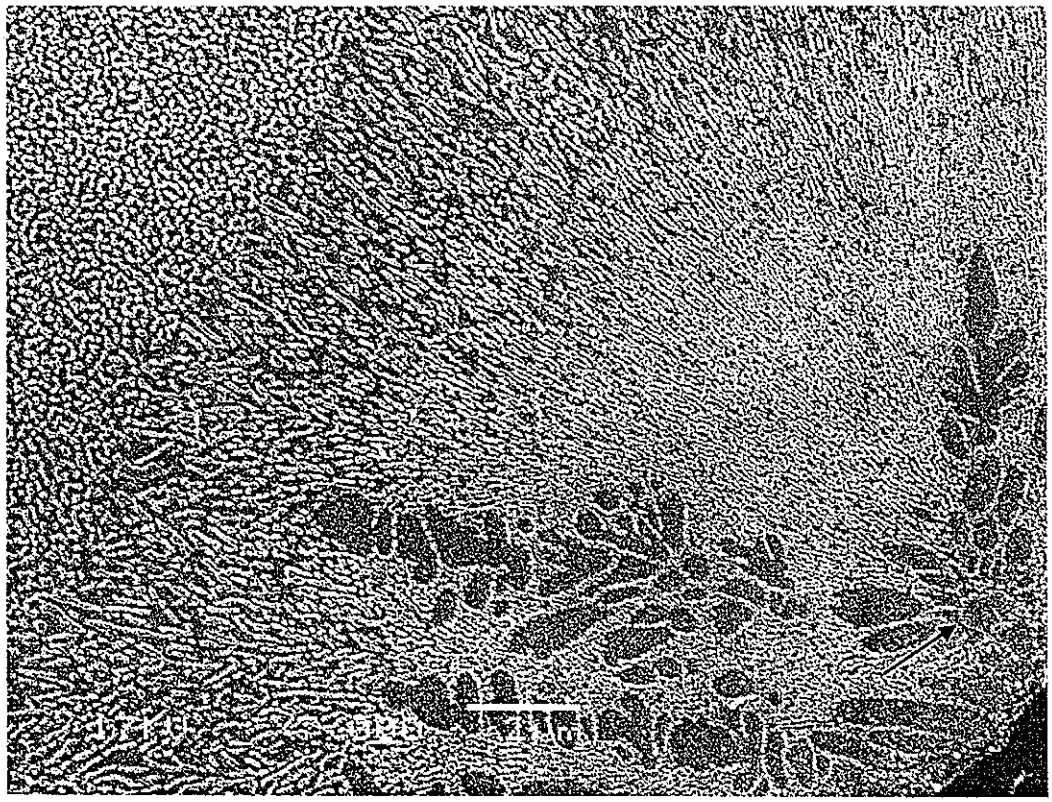

Figure 27. Close up of particle from Figure 25 showing the transition from lamellar to irregular eutectic, as well as the Si crystal nucleus (indicated by arrow). 42 μm diameter, Al-18Si, He atomized. 7,000X

Silicon Crystal Observations

The primary silicon crystals which nucleate at the start of many droplet solidification reactions were measured to be between 0.3 μm and 3.5 μm, with the average size being approximately 1 μm. In any given powder, all the crystals are generally about the same size; however, as with measurement of the particles themselves, it is difficult to determine the true diameters of the crystals from a single, cross-sectional view. As the graph in Figure 28 shows, crystal size increases with increasing particle size as well as, more dramatically, with increasing silicon content. The effect of gas choice is undeterminable without more data because of the scarcity of detectable silicon crystals in the helium atomized Al-15Si.

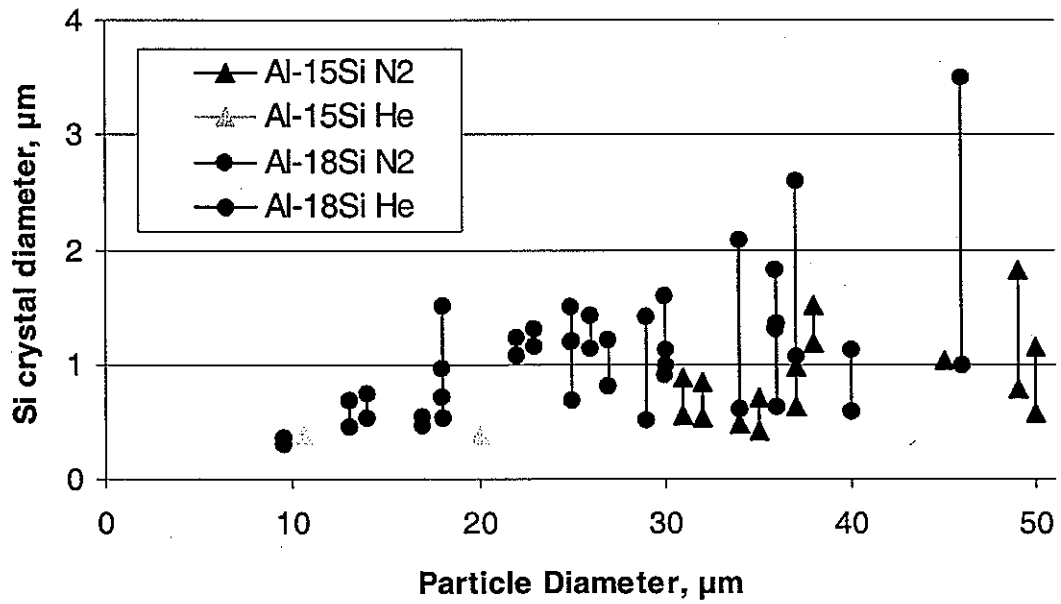

Figure 28. Effect of atomization gas, particle size and composition on size of nucleated silicon crystal particles.

X-ray Diffraction Results

The XRD results on the melt spun ribbon samples showed no sign of glass formation at any composition. All traces showed only sharp, crystalline peaks, as the examples in Figure 29 show. At a wheel speed of 22 m/s, the cooling rate in the melt is higher than that reached by the atomized particles, indicating that no glass formation is likely in the range of compositions being considered in this study. The deep undercooling that is accessible in atomized particles may give some possibility for glass formation, but from the position of the T_o lines indicated on the phase diagram in Figure 6, even at a much higher Si content, the required undercooling for glass formation is probably unattainable in this system. No glassy alloys have been reported in this system [21].

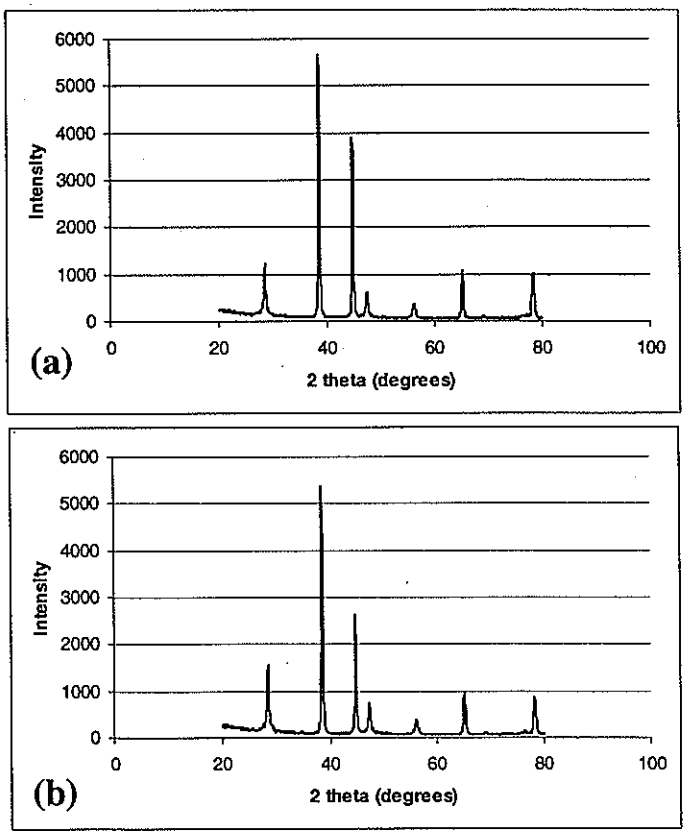

Figure 29. XRD trace for wheel-side (a) Al-25%Si and (b) Al-35%Si, both showing no amorphous regions.

DISCUSSION

Calculation of Velocity and Undercooling

For solidification condition calculations, the eutectic spacing was chosen over the other possible microstructural measurements because eutectic was present and easily measurable in the largest number of particles over the largest size range. The eutectic structure is independent of temperature gradient, so that the eutectic spacing is determined by the magnitude of interface velocity only and can be used to calculate solidification conditions.

As discussed above, the JH model of eutectic growth at low velocities has been extended to high velocities in the TMK model, which relaxes some of the assumptions that do not hold under rapid solidification conditions. At low Peclet numbers, the two models provide similar results, but begin to diverge as rapid solidification conditions are approached. The differences between the undercoolings and velocities predicted for a given spacing by the JH model and the TMK model are illustrated in Figure 30. To be consistent with previous work [31], the deviation in the models was judged to be significant for undercooling values greater than 32 K (spacings < 0.2 μm), and for velocities greater than 0.3 cm/s (spacings < 0.3 μm). From the graphs, the maximum velocity for Al-Si eutectic growth predicted by the TMK model was 6.5 cm/s.

Due to circumstances beyond the control of the author, the TMK calculations were not able to be made in time for inclusion in this thesis. Consequently, all values given below were calculated using the simpler JH model. Since Al-Si has an irregular eutectic, equations (8) and (9) from the JH model were used, where $\text{constant}_1 = 6.89\text{x}10^{-7}$ mm^3/s and $\text{constant}_2 = 8.9\text{x}10^{-3}$ mm·K [31]. As the graphs in Figure 30 show, this will cause the values listed for undercooling to be slightly underestimated, while the velocity values will be slightly overestimated. It should not, however, significantly affect the conclusions which are drawn

from the data. Because of the superiority of the TMK model in this situation, an explanation of the calculation procedure is still included here.

The calculations required for the TMK model are somewhat complicated, but can be accomplished as described below [33]. Like the JH model given in Eq. (1), the TMK model can be written as

$$\Delta T = K_1^{'} \lambda V + \frac{K_2}{\lambda} \tag{15}$$

where

$$K_1^{'} = \frac{mC_o}{f_\alpha f_\beta D} P_{TMK} \tag{16}$$

and K_2 is the same as in the JH model (Eq. 3). By defining a new variable,

$$K_1^{''} = \frac{mC_o}{f_\alpha f_\beta} = K_1^{'} \frac{D}{P_{TMK}} \tag{17}$$

so that K_2 and K_1'' are system constants, the two constants can be simplified as $K = K_2/K_1''$. The TMK relationship for the minimum undercooling is given by

$$V\lambda^2 = \frac{K D}{\left[P + \frac{\partial P}{\partial \lambda}\right]} \tag{18}$$

which can be written as

$$\lambda = \frac{K}{p_c \left[P + \lambda \frac{\partial P}{\partial \lambda}\right]} \tag{19}$$

and used to obtain a relationship between spacing and p_c, the Peclet number, which defined in Eq. 11. The definition of p_c can then be used to calculate the relationship between λ and V according to $V=p_cD/\lambda$, assuming D to be constant. Modifying Eq. 15 by incorporating Eqs. 17 and 18 and the definition of K, the relationship between λ and ΔT can be obtained as

$$\lambda\Delta T = \frac{K_2\, P_{TMK}}{\left[P + \lambda\dfrac{\partial P}{\partial \lambda}\right]} + K_2 \qquad (20)$$

Values for P_{TMK} and $P + \lambda(\partial P/\partial \lambda)$ were obtained from the available tables [19], using the those values where $k_\alpha = k_\beta = 0$. All other values are given in Table 1.

From the spacing measurements shown in Figure 24, the undercooling and velocity of the solid/liquid interface were calculated as a function of average particle size. The results of these calculations are shown in Figure 31, Figure 32, Figure 33 and Figure 34 for the Al-15Si (N_2), Al-15Si (He), Al-18Si (N_2), and Al-18Si (He) respectively. In all four cases, the undercooling is clearly greater in smaller particles. The range in interface velocity also increases as particle size goes down, indicating that the recalescence effect is more pronounced in smaller particles. In much larger particles, those greater than 40 μm in diameter, it has been shown that the recalescence effect becomes almost negligible [7], since the undercooling becomes fairly insignificant.

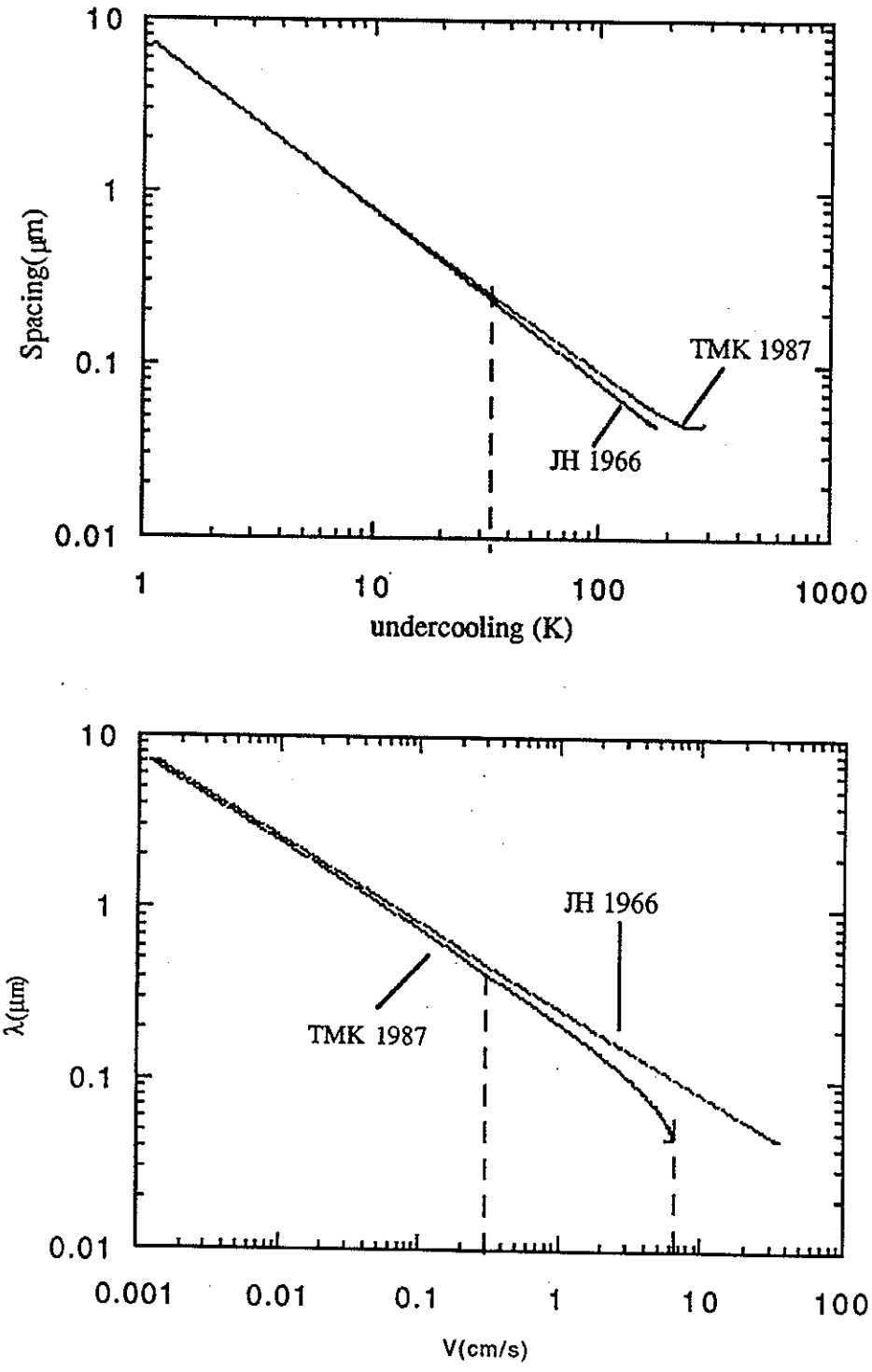

Figure 30. Comparison between calculated results for undercooling between Jackson-Hunt model and TMK model [27].

Table 1. Parameters for the Al-Si System

Parameter Name	Parameter Value
Diffusion Coefficient (D)	5×10^{-9} m^2/s
Length of Eutectic Tie-line (C_o)	98.2 wt%
α Phase Fraction (f_α)	0.866 (15 wt%) 0.835 (18 wt%)
β Phase Fraction (f_β)	0.134 (15 wt%) 0.165 (18 wt%)
α Phase Liquidus Slope (m_α)	7.5 K/wt%
β Phase Liquidus Slope (m_β)	17.5 K/wt%
Gibbs-Thomson Coefficient (Γ_α)	1.96×10^{-7} Km
Gibbs-Thomson Coefficient (Γ_β)	1.7×10^{-7} Km
Angle of α Phase (θ_α)	30°
Angle of β Phase (θ_β)	65°
K_1"	4650 K
K_2	8.85×10^{-7} Km
K	1.90×10^{-10}
Extremum Condition (Φ)	3.2

(a)

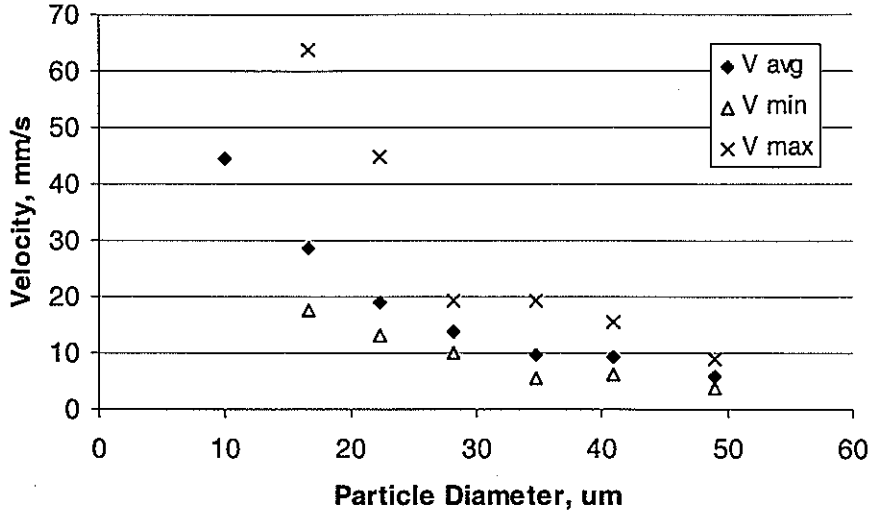

(b)

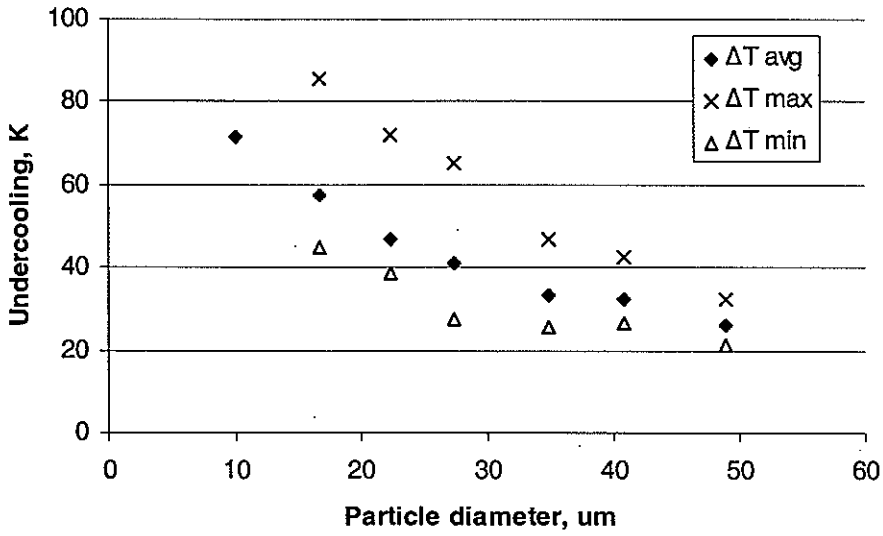

Figure 31. The variations in maximum, minimum and average (a) interface velocity and (b) interface undercooling as a function of particle diameter. Only average data was available for the smallest particle size.
Al-15%Si (N_2)

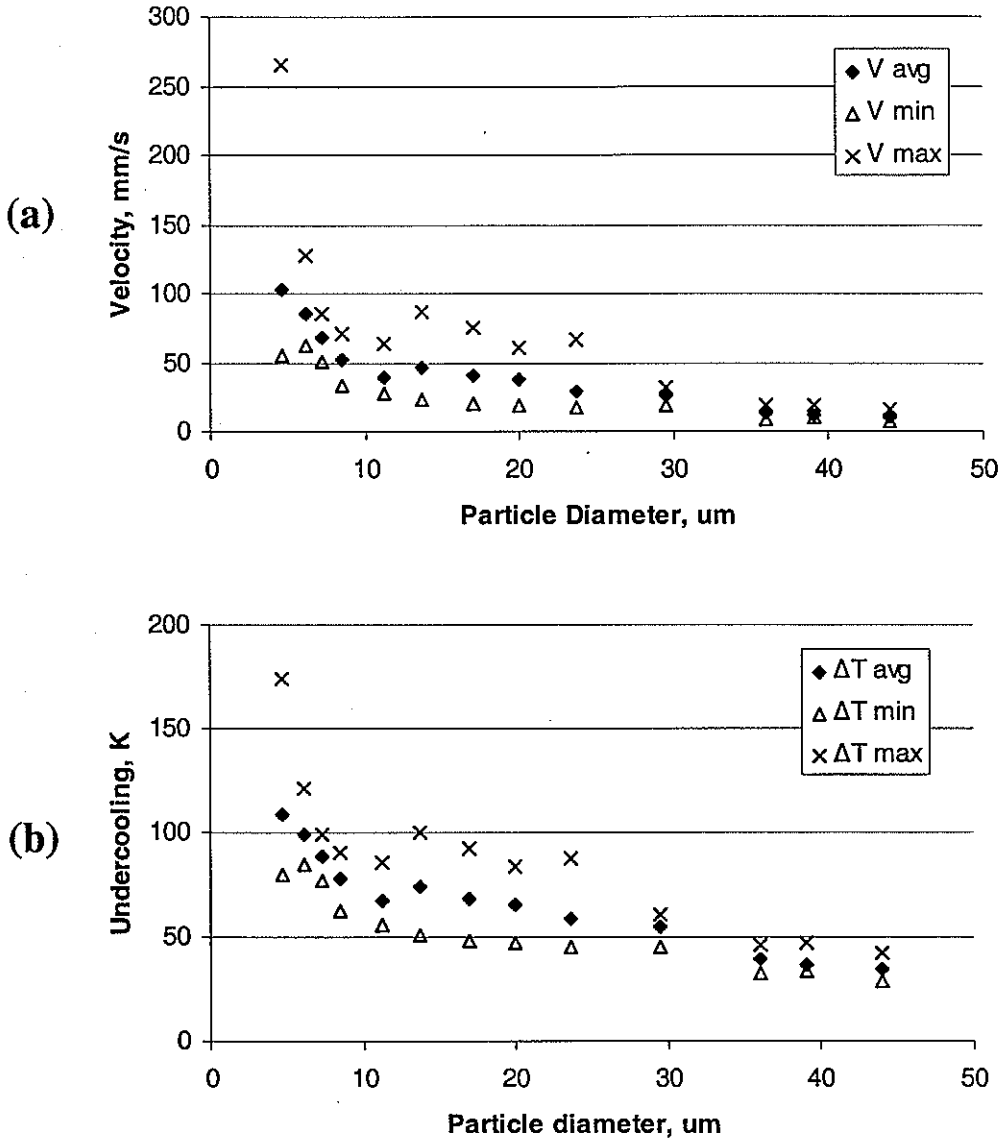

Figure 32. The variations in maximum, minimum and average (a) interface velocity and (b) interface undercooling as a function of particle diameter. **Al-15%Si (He)**

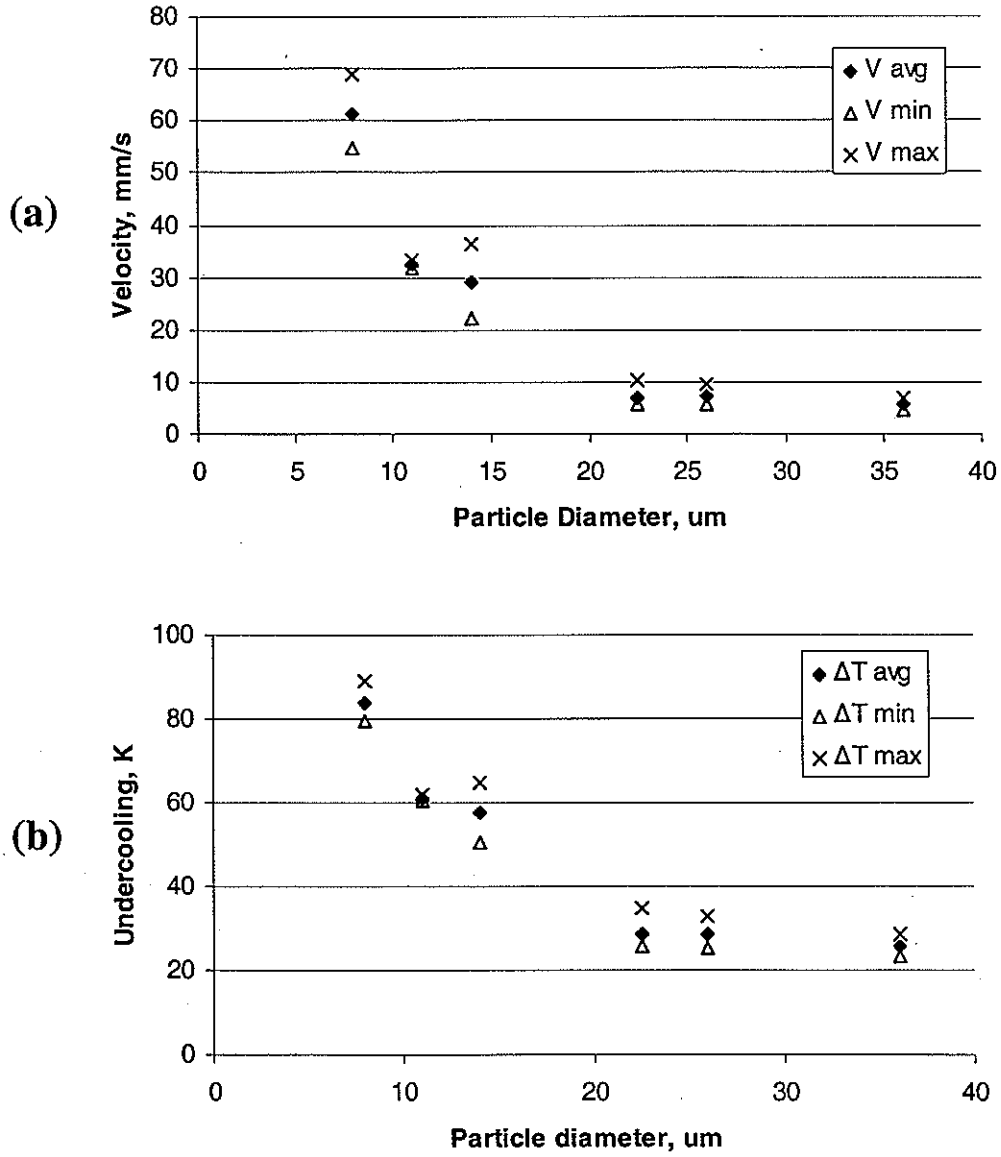

Figure 33. The variations in maximum, minimum and average (a) interface velocity and (b) interface undercooling as a function of particle diameter. **Al-18%Si (N_2)**

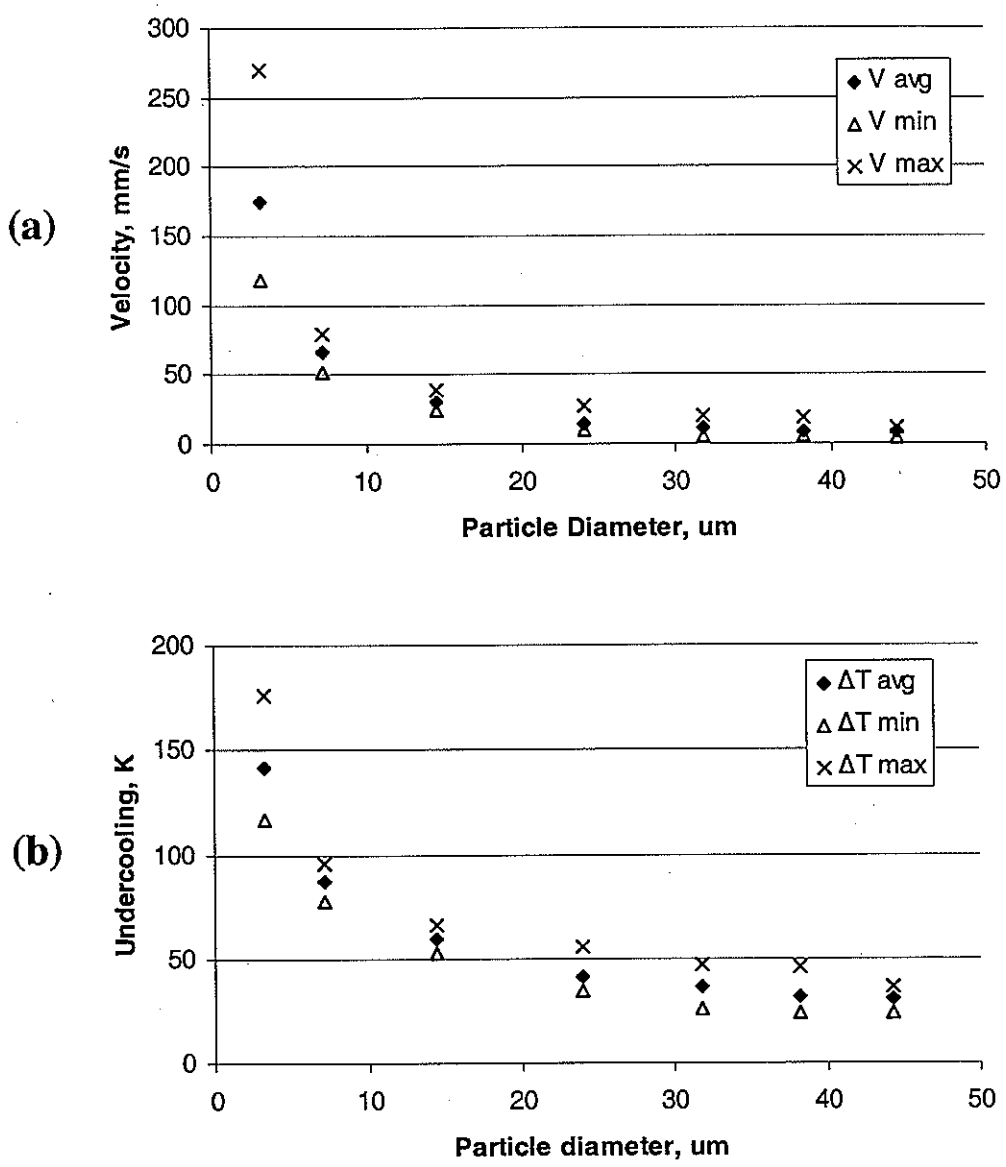

Figure 34. The variations in maximum, minimum and average (a) interface velocity and (b) interface undercooling as a function of particle diameter. **Al-18%Si (He)**

Effect of Atomization Gas and Composition

For comparative purposes, the average undercooling for all four powder batches are graphed together in Figure 35. The maximum calculated undercoolings are shown together in Figure 36. The first item of importance to note from the graphs is that the gas used during atomization does not affect the coupled growth spacing of particles ~11 μm in diameter or less (also apparent from Figure 24). This is attributed to complete, or nearly complete, adiabatic solidification by these particles. In this regime, external cooling rate should have little or no effect on the properties of the particles. According to Figure 3, the hypercooling limit at which complete adiabatic solidification would occur in pure Al alloys is about 300 K. The maximum undercooling calculated for these particles is closer to 200 K, so it is unlikely that they are reaching the true limit. However, it appears that they have reached an effective hypercooling limit at which the powder is unaffected by external factors. This finding could have a significant impact on powder processing, as it would allow producers seeking <10 μm powder to use less expensive, easier to handle gases without affecting the resulting powder. These very fine particles also appear to be unaffected by the 3% change in composition.

The largest particles studied also appear only marginally affected by gas choice. Comparing the Al-15Si powder atomized with helium to the same composition atomized with nitrogen, only a slight increase in average undercooling is obtained from the helium gas, and virtually no change is observed in the maximum undercooling. Note that the average undercooling corresponds to the average interface temperature during solidification, while the maximum undercooling corresponds, as nearly as could be measured, to the undercooling at nucleation. More work is required, including TEM, to find the nucleation sites in more particles and to determine the true nucleation temperatures.

From these results, however, it appears that the abundance of active nucleation sites present in these larger particles cannot be overcome by the increased cooling power of helium, causing the droplets to begin solidification at approximately the same relatively low undercooling. Because recalescence effects are fairly minimal in the larger particles, the

solidification is controlled mainly by external heat extraction ('isothermal' regime [6]). The effect of the increased cooling rate of helium can be seen in the increase in average undercooling values, as the gas pulls heat out of the solidifying droplet faster than nitrogen is able to do, producing a faster interface and maintaining greater undercooling values. This has been verified by new measurements on the N_2 atomized Al-18Si.

As Figure 36 clearly shows, the maximum undercoolings for the Al-15Si particles between 10 and 30 μm are significantly higher than those measured for comparably sized particles with the higher silicon content. This size range corresponds closely to the range in which Al dendrites nucleated without primary Si were observed in the deep etched powder at Al-15Si (N_2). That type of dendrite is not seen at Al-18Si, suggesting that a correlation between the dominant morphology and undercooling exists. Those particles which contained active catalyst sites experienced silicon nucleation, cutting short the undercooling of the droplet. Those droplets with less active sites for silicon nucleation reached the greater undercooling values required for the nucleation of Al dendrites. It appears that this trend is composition based and not dependent on gas type.

In the range of compositions studied, increasing silicon content caused a decrease in the amount of undercooling which occurred before nucleation. This is attributed to an increase in the number of primary silicon crystals which form at the higher silicon content. Further study would be useful to determine how much higher in Si content this trend continues. If there is some heterogeneous nucleation temperature for Al on Si, it would be expected that the amount of undercooling in the particles would stabilize at that temperature when the amount of silicon had increased enough to cause a large number of active Si particles to be present in all the particles. This nucleation phenomenon may be the reason that Pierantoni found mean eutectic spacing not to vary with composition in his laser surface melting experiments [25].

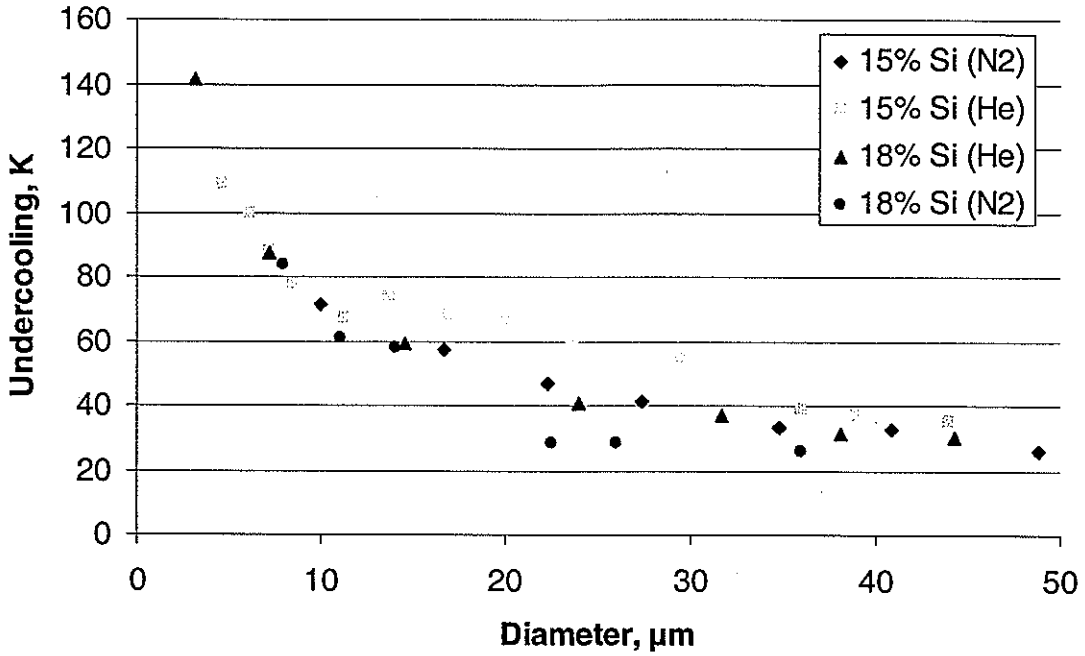

Figure 35. Average undercooling as calculated for all four powder batches.

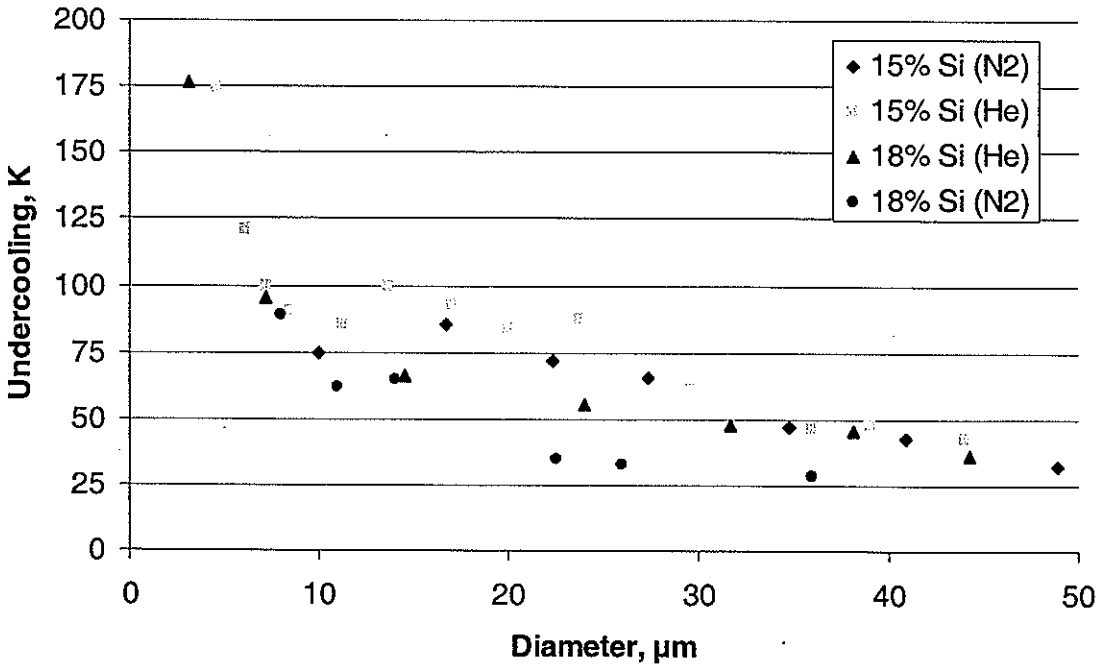

Figure 36. Maximum undercooling as calculated for all four powder batches.

Single Crystal Analysis

The experimental spacing measurements from Figure 26 were used to produce the plots shown in Figure 37. In the single crystal droplet, the interface velocities varied from 12.5 to 1.7 cm/s, and the interface undercooling varied from 122 to 40 K below the eutectic temperature. The decrease in both velocity and undercooling as the particle solidifies is due to heating of the growing interface during recalescence which can not be overcome by the droplet surface cooling process. Extrapolating from the calculated points, a nucleation temperature of 130-140 K is estimated for this particle. Note that this is a very high undercooling for such a large particle, and that single crystal particles such as this are very rare. It does, however, provide an exceptional opportunity for detailed investigation.

A significant decrease in the slope of the line, described by the points in Figure 37(a), occurs at a distance of about 15 μm along the particle and corresponds closely to the change in microstructure indicated by the arrows in Figure 25 at that point. The change is attributed to a transition from adiabatic to isothermal solidification, as described by Levi and Mehrabian [14] and outlined earlier (see page 6).

Gill et. al. [34] calculated that the fraction of the radius of a droplet which is solidified during recalescence (i.e. under adiabatic conditions) is about $S^{1/3}$, where S is the Stefan number, defined as the undercooling multiplied by the heat capacity and divided by the latent heat of fusion. Approximating with property values for pure aluminum and an undercooling of 130 K, the transition is calculated to occur at 71% of the radius. The actual transition occurs 16 μm along the 21 μm radius, or 76%, confirming the source of the change as a transition from internally controlled to externally controlled heat flow. It should be possible to conclude, as well, that the same cause can be attributed to this microstructural transition when it occurs in multi-crystal particles.

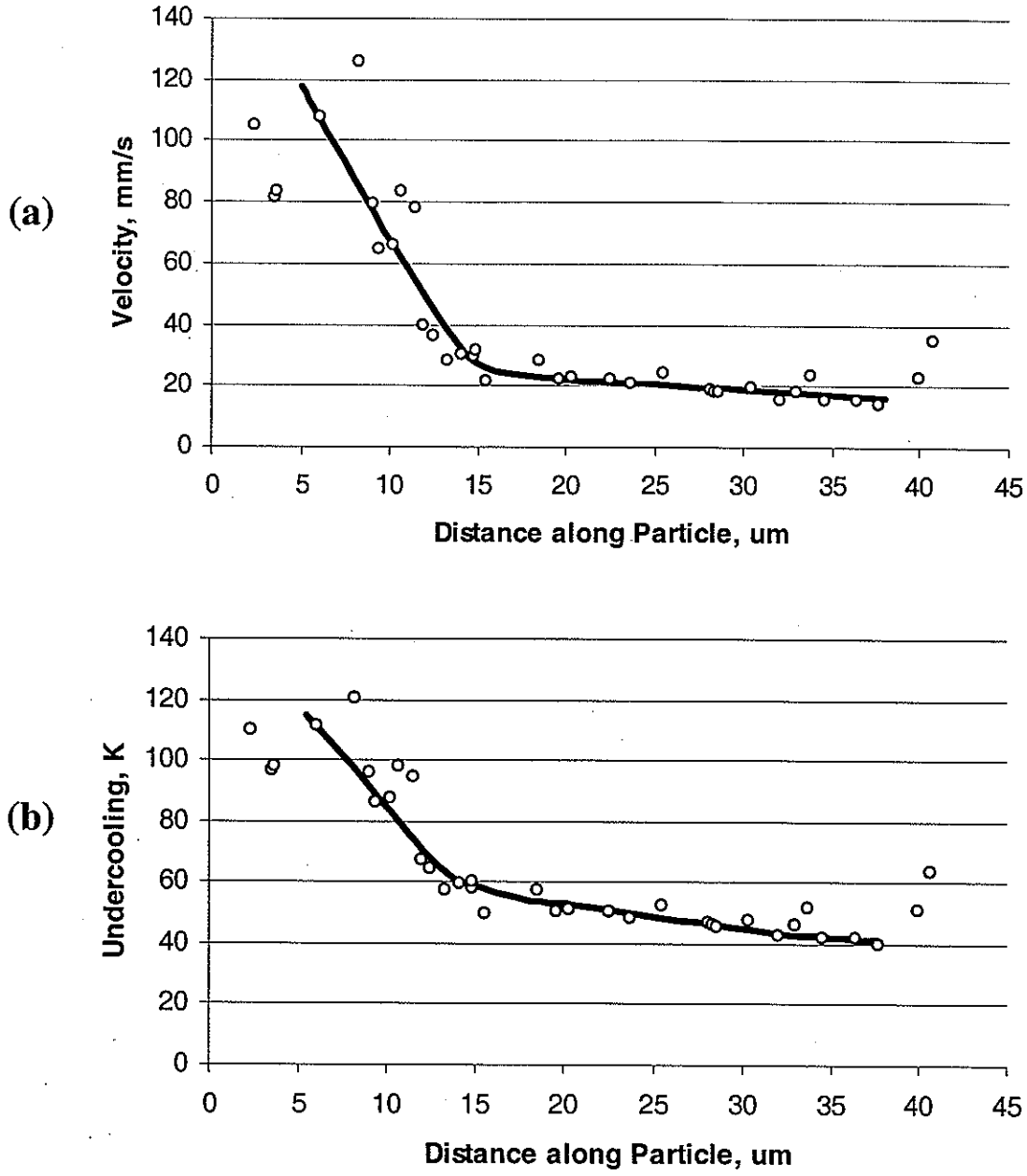

Figure 37. The variations in (a) interface velocity and (b) interface undercooling as a function of distance within a particle of 42 μm diameter, composition Al-18Si.

Revision of Microstructure Map

The undercoolings calculated with the JH model can be used to place particles on the microstructural map shown in Figure 8. However, many of the particles were discovered to cool to temperatures below the bottom of the map. To accommodate these particles, the map was revised, shown in Figure 38, with a sixty degree extension on the bottom. With this extension, it becomes apparent that it is still possible to obtain dendritic aluminum at 18% Si. This requires an undercooling of 110 K below the eutectic temperature. Note that the undercooling calculated from eutectic spacing is the undercooling below the eutectic temperature. As silicon content increases, the actual undercooling as measured from the liquidus line increases as well.

The maximum undercooling obtained, calculated from the spacing of a 3.4 μm particle atomized with He, was 170 K. Due to the model used for calculations and the inherent difficulty in obtaining accurate measurements from the micrographs, an error of at least ±10 K is present in the reported undercooling values. The work of Trivedi, Magnin and Kurz on rapid solidification modeling indicates that the actual undercooling values should be somewhat larger than those calculated with this model.

The tentative line between dendritic and cellular aluminum regions has been shifted downwards by 50 K because of structures that are clearly dendritic showing undercoolings of at least 120 K. More work is required to determine the position and slope of this line with reasonable certainty. No particles that could be conclusively labeled as cellular were identified in this study. This may be due in part to the difficulty in identifying a cellular structure in a three dimensional particle based on a single cross section. Serial sectioning, along with continued study (including TEM) of the <5 μm powders, may help to resolve this issue.

It is interesting to consider whether the map can be pushed to even lower temperatures. Is it possible that, at some point, the particles become truly uniform, having reached a solidification velocity sufficient to produce partitionless solidification, beyond the

absolute velocity limit (path B in Figure 3), where non-equilibrium at the interface must be taken into account [35]. The undercooling required for the interface velocity to reach the critical speed for partitionless solidification is unknown for this alloy system; however, significant increases in available undercooling were seen in the >5 μm particles which were measured, and if the trend continues, undercoolings of well over 200 K should be possible in >1 μm powder. These powders are electron transparent to 200 kV electrons, making analysis by TEM fairly straight forward and an obvious direction for future study. It would also allow a comparison to the EHD-atomized particles which cooled in vacuum [6].

Another possibility for the future study of very fine particles is to look at the effect of particles cooled below the Al T_o line. Figure 39 shows another version of the microstructure map extended another 40 K lower and with the T_o line included. Previous studies of highly undercooled hypoeutectic Al-Si powder have found that it is possible to achieve plane-front partitionless solidification in particles <1 μm [6]. Whether this is possible in hypereutectic compositions is unknown. The metastable Al liquidus line may also have some effect on microstructure evolution in larger particles, and is included in the figure.

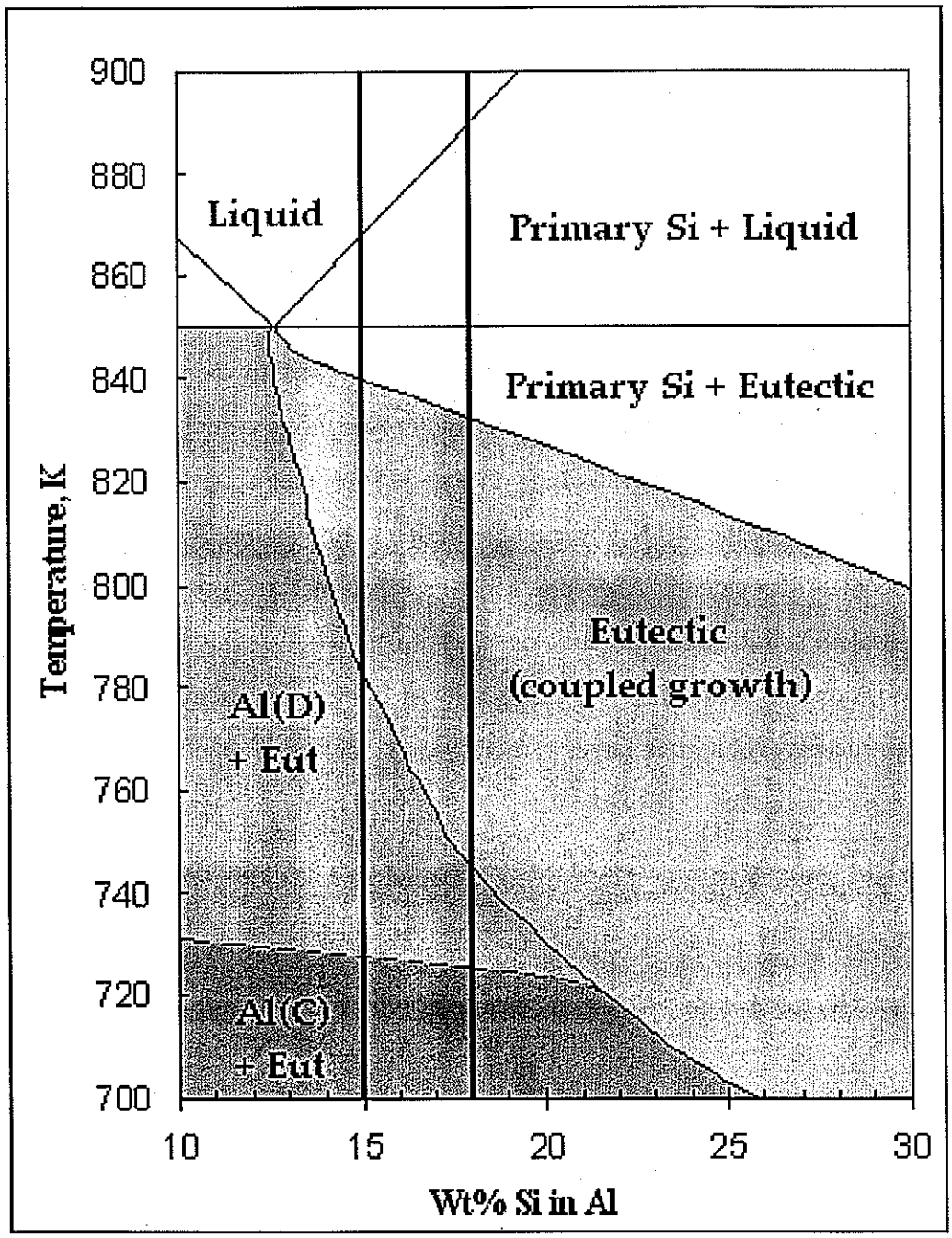

Figure 38. Revised growth morphology map for the Al-Si system.

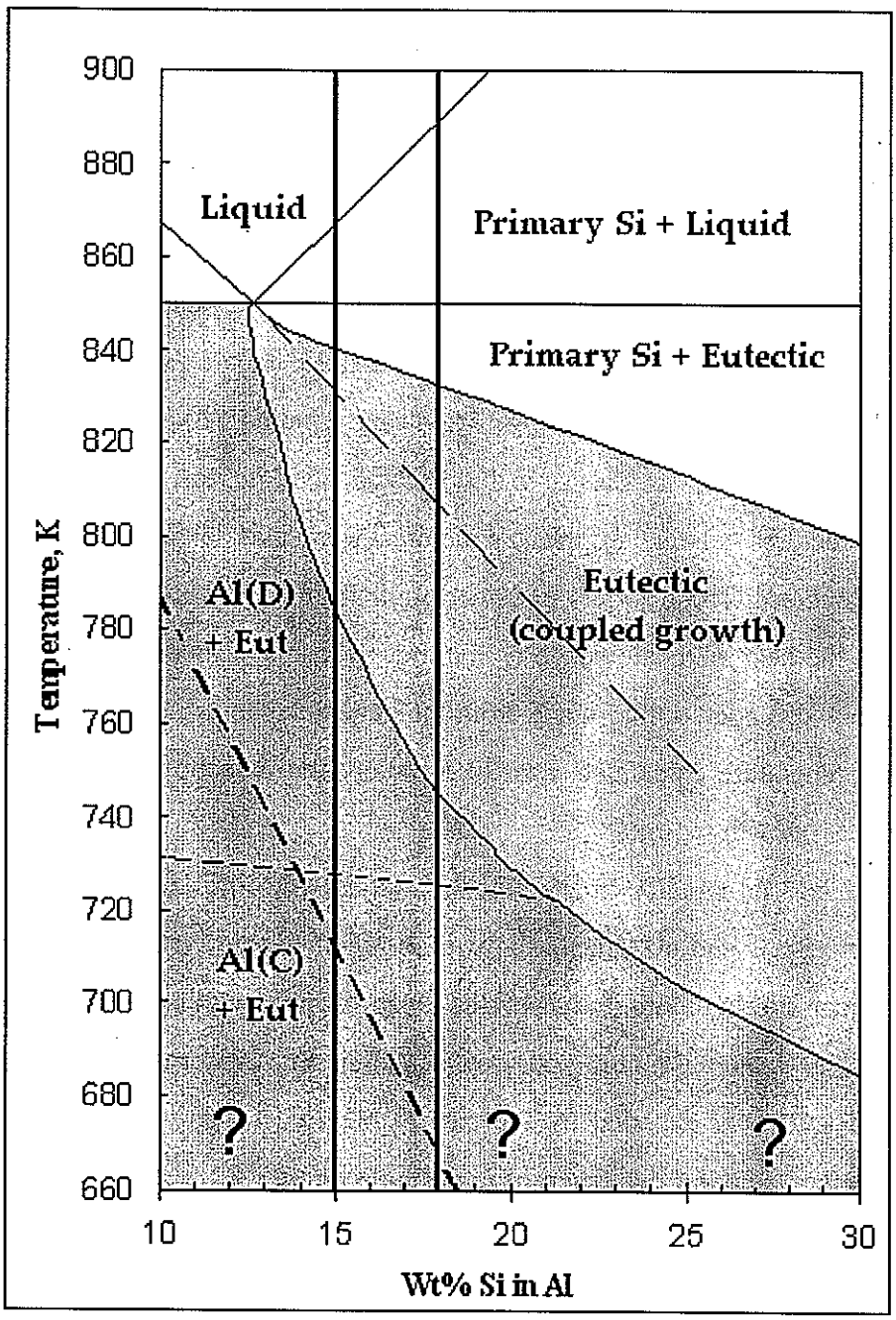

Figure 39. Revised growth morphology map including Al T_o line (black) and metastable Al liquidus extension (red). The uncertainty at very low temperatures is indicated.

Nucleation and Growth Analysis

Combining the results from the JH/TMK analysis with the newly revised microstructure map, a comprehensive explanation of the observed morphologies can be made. After extensive study of the powders, only two true growth patterns were discovered to exist in the observed particles: dendritic/cellular α-Al surrounded by coupled eutectic, and pure coupled eutectic growth. The yellow region of the map, predicting primary silicon surrounded by eutectic, is apparently not accessible, even in the largest atomized droplets studied, within the composition range of powders studied. As discussed in the introduction, primary silicon grows as flakes, plates, faceted dendrites or, at very low velocities, star-shaped structures. None of these structures were ever observed in any of the powder particles studied. The powders undercool initially to substantially below that region of the map, and the heat of recalescence is not enough to move them back into that regime. The calculations of undercooling made from the eutectic spacings support this hypothesis. The highest temperature calculated was 20 K below the eutectic temperature, well below the predicted Si-growth regime.

Of course, small primary silicon crystals were present, but they are the result of nucleation effects and not a stable growth regime. In this system, it is possible to nucleate either silicon or aluminum, based on the composition and conditions within each individual particle. Nucleated aluminum will grow as aluminum cells or dendrites, while the growth of nucleated silicon is impeded by the energy required to grow a faceted surface, and will almost immediately be overtaken by a different phase (Al) nucleating on the surface of the crystal.

Nucleation is possible from the aluminum or mixed (Al-Si) oxide layer surrounding each particle, or from catalytic sites within the particle. The undercooling required for nucleation depends on the type and potency of these sites, which are highly variable, and repeated nucleation experiments have shown that even in a single droplet, nucleation will not always occur at the same temperature [36]. It is, therefore, impossible to accurately predict

the nucleation behavior of an individual particle. However, powder metallurgy deals with millions or billions of particles, not individual ones, and three general trends are observable.

First, the likelihood of nucleating silicon increases with silicon content. At Al-15Si, although it is above the eutectic composition, a substantial fraction of powders avoid silicon nucleation, while at Al-18Si, it appears to be impossible to avoid Si nucleation except possibly in the very finest powders (<5 μm). Second, the probability of nucleating silicon increases with increasing particle size. This is expected, since the "motes" causing Si nucleation are stochastically distributed throughout the droplets during the atomization process, making the smaller droplets less likely to contain them. In the Al-15Si N_2 atomized powder, the only batch showing a complete morphology transition, the largest observed particles show 100% silicon nucleation, the smallest show 100% aluminum nucleation, and the middle size fractions show a mix of nucleation methods, with the number of Si crystals decreasing as diameter decreased. Third, there also seems to be some dependence of nucleation on cooling rate, because Al-15Si powder atomized with He is less likely to show Si nucleation than powder of the same size and composition atomized with N_2.

From these observations, it appears that aluminum is the more difficult of the phases to nucleate, and will only occur if there is a lack of catalytic sites for Si nucleation, permitting sufficient undercooling of the liquid droplet. This is illustrated in Figure 40, which shows schematically the nucleation of the two different phases in a TTT-type diagram. As the diagram shows, at high enough cooling rates, it is possible to avoid Si nucleation in the Al-15Si alloy, while at Al-18Si, the nucleation of Si is unavoidable. Studies of Al-Ge, which has similar properties to Al-Si, have found that primary Al crystals are ineffective in promoting the nucleation of eutectic structure, and that the nucleation of primary Ge is required for the formation of a eutectic structure [30]. A TEM study would be useful to determine the nature of eutectic formation in Al-Si, as well as the nucleation properties of the primary Al phase.

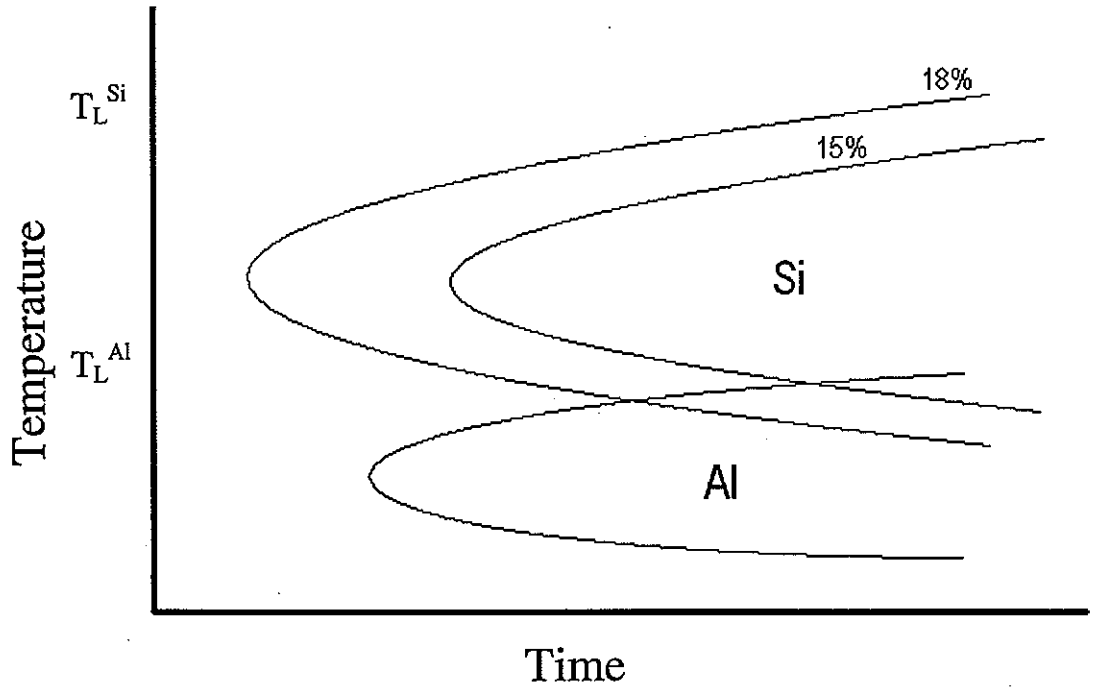

Figure 40. Illustration of nucleation behavior in Al-Si powder.

At 18% Si, those particles which cool into the coupled growth region appear as silicon crystals surrounded by a highly irregular eutectic. Growth appears to emanate from a large number of nucleation sites. There is wide variation in the particles which spacing measurements indicate cooled into the Al(D) region. Some show small, stubby dendrites surrounding primary silicon, while others show dendrites which are narrow, oriented and highly branched growing off similar silicon crystals. The orientation is attributed to the epitaxy between the two phases, mentioned earlier as the <111>/<111> planes. The difference in dendrite size is attributed to undercooling, and hence the amount of growth accomplished before recalescence causes the interface to pass into the coupled growth regime. Preliminary measurements of eutectic spacing near the nucleation site support this hypothesis, but more work with the higher resolution of TEM is needed due to the extreme fineness of the scale.

One phenomenon, observed only in the Al-18Si powder and believed to be previously unreported, is extreme refinement of eutectic spacing observed at colony boundaries. Judging from the spacing variation, the decrease in the interface velocity caused by recalescence is followed by a sudden and extreme increase in velocity as the interfaces impinge on each other, for which no good explanation has been found. A partial explanation may be the variation in interface composition due to solute buildup. Some dimensional effect not apparent in cross sectional views is also a possible cause. Creating a three dimensional model of the irregular eutectic growth which occurs in these particles may provide answers to this question, and other questions raised here, and is one intriguing possibility for future work in this area.

The growth structures observed present exciting possibilities for industrial applications as well. This study has shown that it is possible to produce Al-15Si powder up to at least 45 μm which contains classic aluminum dendrites and eutectic with virtually no primary silicon, simply by atomizing with helium gas. This should provide a measure of ductility in applications where powder compressibility is important. At the other extreme, by increasing the silicon content to 18%, powder can be obtained which is mostly an extremely fine coupled eutectic with minimal dendrite growth and no primary silicon larger than 3.5 μm. Powder of this type should provide exceptional strength and toughness.

CONCLUSIONS

The effects of composition, particle size and atomization gas on particle microstructure were analyzed for two hypereutectic Al-Si alloys processed by high pressure gas atomization. Analysis of deep etched loose powder and etched cross sections of mounted powder was carried out to determine what trends in nucleation and morphology evolution exist.

Two types of growth were observed: cellular/dendritic α-aluminum (distinction between cells and dendrites was difficult) surrounded by eutectic; and pure coupled eutectic. In very fine (<4 μm) Al-15Si powder atomized with He, a single phase interdendritic region was observed, but is likely due to coarsening of an extremely fine coupled phase. The growth of primary silicon beyond very small faceted crystals (1-3 μm in diameter) was never observed.

The appearance of these basic microstructures were substantially affected by the type of nucleation which occured. Three types of nucleation were observed: primary Si crystals nucleating first, with Al nucleating off the Si; Al cells/dendrites nucleating without Si; and nucleation off external or internal inclusions. Nucleation of primary silicon can be minimized by decreasing silicon content, decreasing particle size, and by atomization with He (compared to N_2).

Eutectic spacing measurements were made from cross sectional images of the powder particles. The Jackson-Hunt model and Trivedi-Magnin-Kurz model were used to calculate interface velocity and undercooling from the eutectic spacing measurements. Variations in morphology can be linked to changes in both maximum undercooling and average undercooling. Atomization with helium provides noticeably finer powder, along with generally higher undercoolings and faster interface velocities. Gas choice does not, however, affect the solidification of particles 11 μm or below due to compete adiabatic solidification of these particles.

From the analysis of a large, apparent single crystal particle, it was determined that the transition from adiabatic to isothermal solidification is visible as a transition from oriented to non-oriented coupled eutectic growth.

The proposed microstructural growth map from previous work has been revised to reflect the new data which is available from this study. The map was extended downward to reflect the high levels of undercooling which were calculated, and the cellular/dendritic boundary was shifted downward to reflect the reality that cellular structures require more undercooling than previously supposed.

Studying the solidification of atomized powder presents a difficult problem. Competing effects of nucleation and growth, as well as effects of the atomization process and the inability to directly measure solidification conditions within the atomizer, make the solidification of these droplets a complex process. However, the unique properties made possible by atomization, and their potential to positively impact metal processing techniques on an industrial scale, make it a worthwhile endeavor. This is an area in which more study is critically needed.

REFERENCES

1. S.S. Cho, B.S. Chun, C.W. Won, H.K. Kim, B.S. Lee, K. H. Yim, S.H. Eom, H. Baek, B.J. Song, and C. Suryanarayana: "Microstructure and mechanical properties of rapidly solidified hypereutectic Al-Si and Al-Si-Fe alloys" *J. Materials Synthesis and Processing*, 1998, vol. 6, no. 2, p. 123-131.

2. R. Terpstra. Private Communication. June 17, 2004.

3. I.E. Anderson and R.L. Terpstra: "Progress toward gas atomization processing with increased uniformity and control" *Mat. Sci. Eng.*, A326, 101 (2002).

4. I.E. Anderson, R.L. Terpstra, S. Rau, and R. Figliola: "Increased understanding of gas atomization from gas flow imaging and high speed cinematography" *JOM*, 2002, vol. 54, p. 6.

5. I.E. Anderson, R.S. Figliola, R.L. Terpstra, S. Rau, and B. Rauscher: "Progress in experimental analysis of gas atomization process physics" in *Advances in Powder Metallurgy and Particulate Materials — 2002*, compiled by V. Arnhold, C.-L. Chu, W.F. Jandeska, Jr., H.I. Sanderow, Metal Powder Industries Federation, Princeton, NJ, 2002, p. 3-150 to 3-162.

6. C.G. Levi and R. Mehrabian: "Microstructures of rapidly solidified aluminum alloy submicron powders" *Metall. Trans.*, 1982, vol. 13A, p. 13-23.

7. R. Trivedi, F. Jin and I.E. Anderson: "Dynamical evolution of microstructure in finely atomized droplets of Al-Si alloys" *Acta Mater.*, 2003, vol. 51, p. 289-299.

8. S.-J. Hong and C. Suryanarayana: "Mechanical properties and fracture mechanism of nanostructured Al-20wt%Si alloy" in *Processing and Properties of Structural Nanomaterials*, Mater. Sci. and Tech., Chicago, IL, 2003, p. 133-140.

9. J.D. Ayers and I.E. Anderson: "Method for generating fine sprays of molen metal for spray coating and powder making" U.S. Patent No. 4,619,845. October 28, 1986.

10. W.J. Bottinger and J.H. Perepezko: in *Rapidly Solidified Crystalline Alloys*, S.K Das, B.H. Kear, C.M. Adam, eds., TMS-AIME, Morristown, NJ, 1985, p. 21.

11. I.E. Anderson and M.P. Kemppainen: "Undercooling effects in gas atomized powders" in *Undercooled Alloy Phases*, E.W. Collings and C.C. Koch, eds., TMS-AIME, New Orleans, 1986, p. 269-285.

12. R. Mehrabian: in *Rapid Solidification Processing, Principles and Technologies*, R. Mehrabian, B.H. Kear, and M. Cohen, eds., Baton Rouge, 1978, p. 246.

13. I.E. Anderson and B.B. Rath: "Rapid solidification of copper-based alloys" in *Rapidly Solidified Crystalline Alloys*, S.K. Das, B.H. Kear, and C.M. Adam, eds., TMS-AIME, Morristown, NJ, 1985, p. 219-244.

14. C.G. Levi and R. Mehrabian: "Heat flow during rapid solidification of undercooled metal droplets" *Metall. Trans.*, 1982, vol. 13A, p. 221-234.

15. K.A. Jackson and J.D. Hunt: "Lamellar and rod eutectic growth" *Trans. Met. Soc. AIME*, 1966, vol. 236, p. 1129-1142.

16. W. Kurz and D.J. Fisher: *Fundamentals of Solidification*, Trans. Tech. Publications, 1984.

17. R. Trivedi and W. Kurz: in *Solidification Processing of Eutectic Alloys*, D.M. Stefanescu, G.J. Abbaschian and R.J. Bayuzik, eds., TMS, Warrendale, PA, 1988, p. 3.

18. H. Jones and W. Kurz: *Z. Metallkde.*, 1981, vol. 72, p. 792.

19. R. Trivedi, P. Magnin and W. Kurz: "Theory of eutectic growth under rapid solidification conditions" *Acta Metall.*, 1987, vol. 35, p. 971-980.

20. W. Kurz and R. Trivedi: "Eutectic growth under rapid solidification conditions" *Metal. Trans.*, 1991, vol. 22A, p. 3051-3056.

21. J.L. Murray and A.J. McAlister: *Binary Alloy Phase Diagrams*, T. B. Massalski, H. Okamoto, P.R. Subramanian and L. Kacprzak, eds., 1990, vol. 1, 2nd edition, p. 211-213.

22. Y. Birol: "Microstructural characterization of a rapidly solidified Al-12wt%Si alloy" *J. Mater. Sci.*, 1996, vol. 31, p. 2139-2143.

23. Z. Wang, F. Guo, H. Yu, C. Cao and B. Wei: "Rapid solidification of Al-18%Si hypereutectic alloy in drop tube" *Trans Nonferrous Met. Soc. China*, 2000, vol. 10, no. 6, p. 769-771.

24. T.S. Kim, B.T. Lee, C.R. Lee and B. Chun: "Microstructure of rapidly solidified Al-20Si alloy powders" *Mater. Sci. Eng.*, 2001, vol. A304-306, p. 617-620.

25. M. Pierantoni, M. Gremaud, P. Magnin, D. Stoll and W. Kurz: "The coupled zone of rapidly solidified Al-Si alloys in laser treatment" *Acta Metall. Mater.*, 1992, vol. 40, no. 7, p. 1637-1644.

26. O.A. Atasoy, F. Yilmaz and R. Elliot: *J. Cryst. Growth*, 1984, vol. 66, p 137.

27. B.A. Mueller, L.E. Tanner and J.H. Perepezko: "Microstructure development in undercooled Al-Be powders" *Mater. Sci. Eng.*, 1992, vol. A150, p. 123-132.

28. L.A. Bendersky, F.S. Biancaniello, S.D. Ridder and A.J. Shapiro: "Microstructural characterization of atomized powder of Al-5Mn-5Fe-2Si (wt%) alloy" *Mater. Sci. Eng.*, 1991, vol. A134, p. 1098-1102.

29. I.E. Anderson, R.L. Terpstra, and R. Figliola: "Gas recirculation flow in the melt feeding zone of a close-coupled gas atomization nozzle: Modeling and Measurement" in *SDMA 2003, 2nd International Conference on Spray Deposition and Melt Atomization* and *ICSF V, 5th International Conference on Spray Forming*, K. Bauckhage, U. Fritsching, V. Uhlenwinkel, J. Ziesenis, and A. Letham, eds., Universität Bremen, Germany, 2003, p. 2-19.

30. C. Lemaignan: "Initial stages of eutectic solidification" *Acta Metall.*, 1981, vol. 29 p. 1379-1384.

31. F. Jin: "Microstrucural development of rapid solidification in Al-Si powder" M.S. Thesis, Iowa State University, 1995.

32. *Metals Handbook: Metallography, Structures and Phase Diagrams*, vol. 8, 8th ed., American Society for Metals, Metals Park, OH, 1973, p. 41.

33. R. Trivedi, Private Communication. June, 2004.

34. W.N. Gill, J. Jang, J.C. Mollendorf and C.M. Adam: "Rapid solidification of subcooled small metallic drops: internal nucleation" *J. Cryst. Growth*, 1984, vol. 66, p. 351-368.

35. W.J. Boettinger and S.R. Coriell: in *Rapid Solidification Processing, Principles and Technologies*, R. Mehrabian, ed., Gaithersburg, MA, 1982, p 44.

36. M.J. Uttormark, J.W. Zanter, J.H. Perepezko: "Repeated nucleation in an undercooled aluminum droplet" *J. Cryst. Growth*, 1996, vol. 177, p. 258-264.

ACKNOWLEDGEMENTS

I would like to extend my most sincere thanks to my advisor, Iver Anderson. His knowledge, support and unbridled enthusiasm have been inspirational. Thanks also to my committee members, Rohit Trivedi and Pal Molian. Dr. Trivedi has been especially helpful, providing guidance and direction during the many discussions in which he lent his vast knowledge to this project. He also provided the calculation routine used to determine undercoolings and velocities with the TMK model.

My thanks also go out to everyone at Ames Lab who contributed to the work done for this thesis and for helped me to navigate the maze that is a government lab: Bob Terpstra, for his help and moral support every step of the way; Hal Sailsbury, for his metallographic expertise; Fran Laabs, for his help with the SEM (and the venison); Dave Garbett and Hal who preformed the atomization runs; Kevin Dennis who performed the XRD and the ill-fated thermal analysis work; and finally Susan Elsner and Anne Coffman, who always knew the answer to everything. I genuinely appreciate the helpfulness and friendliness of everyone I have interacted with at Ames Lab.

Chris Baker, my undergraduate hourly, was instrumental in the sample preparation and most of the spacing measurements. I stand in awe of his polishing skills. Huge thanks to Chris, as well as Thing 1 and Thing 2 (Tom Ocken and Joel Rieken), for working so hard to get the final powder run done on time. Nick Buelow is awarded a gold star for being a terrific officemate.

This work was performed at Ames Laboratory under Contract No. W-7405-Eng-82 with the U.S. Department of Energy. The United States government has assigned the DOE Report number IS-T 2447 to this thesis.